

1 **On the role of tropical ocean forcing of the persistent**
2 **North American west coast ridge of winter 2013/14**

3 RICHARD SEAGER* AND NAOMI HENDERSON

4 *Lamont Doherty Earth Observatory of Columbia University, Palisades, New York*

* *Corresponding author address:* Richard Seager, Lamont Doherty Earth Observatory of Columbia University, 61 Route 9W., Palisades, NY 10964. Email: seager@ldeo.columbia.edu

Submitted to *J. Climate* February 2016, revised June 2016, August 2016, LDEO Contribution Number xxxx.

ABSTRACT

6 The causes of the high pressure ridge at the North American west coast during winter
7 2013/14, the driest winter of the recent California drought, are examined. The ridge was
8 part of an atmosphere-ocean state that included anomalies, defined as relative to a 1979
9 to 2014 mean, of circulation across the northern hemisphere, warm sea surface temperature
10 (SST) in the tropical west and northeast Pacific and the south Indian Ocean and cool
11 SST in the central tropical Pacific. The SST anomalies differ sufficiently between data
12 sets that, when used to force atmosphere models, the simulated circulation anomalies vary
13 notably in realism. Recognizing uncertainty in the SST field, we use idealized tropical
14 SST anomaly experiments to identify an optimal combination of SST anomalies that forces
15 a circulation response that best matches observations. The optimal SST pattern resembles
16 that observed but the associated circulation pattern is much weaker than observed suggesting
17 an important but limited role for ocean forcing. Analysis of the equilibrium and transient
18 upper troposphere vorticity balance indicates that the SST forced component of the ridge
19 arose as a summed effect of Rossby waves forced by SST anomalies across the tropical Indo-
20 Pacific Oceans and drive upper troposphere convergence and subsidence at the west coast.
21 The ridge, in observations and model, is associated with northward and southward diversion
22 of storms. The results suggest that tropical Indo-Pacific Ocean SSTs helped force the west
23 coast ridge and drought of winter 2013/14.

1. Introduction

California experienced four consecutive drier than normal winters from 2011/12 to 2014/15 which pushed the state into a record multiyear drought that has had serious social, economic, environmental and agricultural consequences (Howitt et al. 2014). Although intensified by long term warming and coincident high temperatures (Williams et al. 2015), the root cause of the drought has been higher than normal pressure at the west coast of North America which has gone along with fewer than normal winter storms bringing precipitation to California (Herring et al. 2014; Swain et al. 2014; Wang and Schubert 2014; Funk et al. 2014; Hartmann 2015; Seager et al. 2015). In an analysis of ensembles of SST-forced simulations conducted with seven atmosphere models by 5 institutions, Seager et al. (2015) provided evidence that in each of the 2011/12, 2012/13 and 2013/14 winters the west coast ridge and decreased precipitation had important contributions from forcing by global sea surface temperature (SST) anomalies, relative to a January 1979 to April 2014 climatological mean. Winter 2011/12 was a La Niña event and hence the anomalous high pressure over the northeast Pacific and dry conditions in southwest North America were akin to the canonical response to La Niña events as in Seager et al. (2014a). Winters 2012/13 and 2013/14 were different and formally El Niño- Southern Oscillation (ENSO)-neutral. Despite this, the SST-forced models still tended to produce a west coast ridge and dry conditions at the coast, including California, but with both of weaker amplitude than observed. Seager et al. (2015) argue that the ridge was partially forced by the tropical oceans via a mode of SST-forced variability, albeit one that explained less variance than ENSO or Pacific decadal variability. The SST-forced mode they identified had a west coast ridge associated with an increased SST gradient across the Pacific Ocean with warm anomalies in the western equatorial Pacific and weak cool anomalies in the central to eastern equatorial Pacific. This SST pattern seemed capable of exciting waves that propagated northeast to place a ridge at the North American west coast. However they also made clear that SST-forcing could not fully explain the west coast ridge nor the associated precipitation reduction and that internal atmosphere variability was likely to have been at least as important.

Since the winter of 2013/14 considerable work has been done to try to explain the causes

53 of the unusual weather across the northern hemisphere. Hartmann (2015) came to a similar
54 conclusion as Seager et al. (2015) based on observational and model analysis and Davies
55 (2015) also did via a potential vorticity analysis of transient weather systems. Lee et al.
56 (2015) showed that many features of the observed circulation anomaly could be reproduced
57 within an atmosphere model forced by the SST and sea ice anomalies that prevailed during
58 the winter arguing for roles for tropical, extratropical and subpolar forcing. On the other
59 hand Baxter and Nigam (2015) showed how the observed circulation anomalies could be
60 understood in terms of known patterns of variability such as the West Pacific-North Pacific
61 Ocean mode and argued for an origin in terms of internal mid-latitude variability. They
62 criticized Seager et al. (2015) for “succumbing to the post 1980s-90s temptation” of ascribing
63 Pacific-North America variability to tropical sources and, together with Hartmann (2015),
64 for failing to provide “process-level observational support” via, for example, analysis of
65 outgoing longwave radiation or diabatic heating. Succumbing to temptation is not always
66 a bad move and can lead to positive outcomes. Watson et al. (2016), in a modeling and
67 observational study, showed that the warm SST anomalies in the tropical west Pacific Ocean
68 did indeed correspond to positive precipitation anomalies (and therefore diabatic heating)
69 and showed that this was one, but by no means the only, process at play in generating the
70 west coast ridge of winter 2013/14.

71 The work performed to date has pointed to answers in regard to generation of the west
72 coast ridge that forced the California drought but leaves many questions unanswered. The
73 current work extends beyond the prior work in terms of examining the physical processes
74 involved in generating the SST-forced component of the ridge. For example, one leading
75 question is: if we accept a limited role for ocean forcing, which we do, where is it in the global
76 ocean that the forcing for the ridge originates and is one region with a simple wave response
77 (e.g. the tropical west Pacific) or multiple regions with superimposed or interacting waves
78 responsible? What were the anomalies in the location and intensity of precipitation-bearing
79 North Pacific storm track associated with the ridge? What are the physical mechanisms
80 of wave-mean flow-transient eddy interaction that connect the SST anomalies to the west
81 coast ridge and suppression of precipitation? Further, once the culprit ocean state has been
82 identified, what ocean-atmosphere processes were responsible for creating that state? Here

83 we will address the first three questions and leave the fourth oceanographic question aside
84 while noting that for the general problem of drought far less attention is paid to the causes
85 of the responsible SST anomalies than to the atmospheric response to them.

86 Here we report on a series of modeling experiments designed to understand the non-
87 ENSO ocean forcing contribution to the west coast ridge focusing in on winter 2013/14 as
88 the more extreme of the two years that had this feature. Given the results in Seager et al.
89 (2015) we can only hope to explain the component of the west coast ridge in winter 2013/14
90 that was SST-forced and not its entirety. It is found here that the usual methodology to
91 identify ocean forcing of imposing actual SST anomalies by ocean basin and region in order
92 to locate the prime forcing region for the response feature of interest does not work well for
93 the case of winter 2013/14. Reasons for this are discussed and in part relate to uncertainties
94 in the SST field itself that may have affected the model-based analyses by the prior workers
95 mentioned above. Recognizing this we turn to a series of idealized SST forcing experiments
96 and use an optimization procedure to identify the combination of tropical SST and associated
97 diabatic heating forcing that leads to the best match for the observed circulation anomaly.
98 The implied SST and precipitation anomalies are compared to those observed and linearity
99 is assessed by rerunning the model forced by the optimal SST forcing pattern. The modeling
100 experiments implicate a collection of SST anomalies in the Indian and tropical Pacific Oceans
101 as combining to help force the west coast ridge and drought of winter 2013/14. We then
102 study the observed and modeled upper troposphere vorticity balance to understand the
103 physical mechanisms that underlay the persistent west coast ridge. To complete the study
104 we then analyze the transient day-by-day and week-by-week adjustment of the atmospheric
105 circulation and vorticity balance in response to the switch-on of the optimal SST forcing
106 field, allowing cause and effect to be successfully diagnosed. By design, the optimization
107 methodology determines an upper bound on the SST-forced contribution to the ridge. Even
108 so, this is weaker than observed. Analysis of the ensemble members supports the idea that
109 internal atmosphere variability combined with the SST-forcing to determine the amplitude
110 and pattern of this extreme event.

2. Observational data and model simulations

a. Observations

For anomalies in the atmospheric circulation during winter 2013/14 we use the National Centers for Environmental Prediction-National Center for Atmospheric Research (NCEP-NCAR) Reanalysis (Kistler et al. 2001) accessed via the International Research Institute for Climate and Society (IRI) Data Library at <http://iridl.ldeo.columbia.edu/expert/SOURCES/.NOAA/.NCEP-NCAR/.CDAS-1/.MONTHLY/> and the European Centre for Medium Range Weather Forecasts Interim Reanalysis (ERA-Interim, Berrisford et al. (2011b,a); Dee et al. (2011), downloaded from <http://www.ecmwf.int/en/research/climate-reanalysis/era-interim>). To analyze global precipitation we use the satellite-gauge data from both the Global Precipitation Climatology Project (GPCP) (Adler et al. 2003) also accessed from the IRI Data Library at <http://iridl.ldeo.columbia.edu/SOURCES/.NASA/.GPCP/.V2p2/.satellite-gauge/> and the Climate Prediction Center Merged Analysis of Precipitation (CMAP, Huffman et al. (1997); Adler et al. (2003)) accessed from the IRI Data Library at <http://iridl.ldeo.columbia.edu/SOURCES/.NOAA/.NCEP/.CPC/.MergedAnalysis/.monthly/.latest/.ver2/>. The most recent issues of each precipitation data were used. For SST we analyzed the Hadley Center HadISST data product (Rayner et al. (2003), accessed from <http://www.metoffice.gov.uk/hadobs/hadisst/data/download.html>), the National Oceanic and Atmospheric Administration (NOAA) Extended Reconstructed SST version 4 data (ERSSTv4, Huang et al. (2015), accessed from <http://iridl.ldeo.columbia.edu/SOURCES/.NOAA/.NCDC/.ERSST/.version4/>) and the European Centre for Medium Range Weather Forecasts (ECMWF) Ocean Reanalysis (ORAS4) of Balmaseda et al. (2013) accessed from <https://reanalyses.org/ocean/overview-current-reanalyses>. Surface latent and sensible heat flux data are from Yu et al. (2008), accessed from <http://oaf Flux.whoI.edu/data.html>, and make use of surface and satellite information and are referred to here as the OA fluxes. All monthly anomalies are relative to a January 1979 to April 2014 climatology.

The atmosphere model we use is the NCAR Community Climate Model 3 (CCM3, Kiehl et al. (1998)) run at T42 resolution with 19 vertical levels. CCM3 is a vintage model but has been the workhorse model at Lamont for over a decade and found to compare favorably

140 with the more recent CAM models for simulation of tropical forcing of North American
141 hydroclimate. Since CCM3 also uses about one twentieth the computing time of the CAMs,
142 allowing for large ensembles and numerous experiments, we will use the vintage CCM3
143 once more here. It was used for the 16 member, 1856 to current, SST-forced ensembles,
144 the analysis of which have led to considerable advances in understanding North and South
145 American drought history (Seager et al. 2005, 2009, 2010a) and has also been applied to
146 understanding the evolution of transient eddy-mean flow interaction over the Pacific-North
147 America region during ENSO events (Seager et al. 2010b). The sensitivity of the atmospheric
148 responses to different observed estimates of the DJF 2013/14 SST anomaly was also assessed
149 with the NCAR Community Atmosphere Model 5 (CAM5.3) also run at T42 resolution with
150 30 levels.

151 We conduct two types of modeling experiment:

- 152 i. 100 member ensembles forced by historical observed SST anomalies during December
153 2013 to February 2014 were generated using different SST data sets as forcing. The
154 ensemble mean is analyzed as an anomaly relative to the January 1979 to April 2014
155 climatology of a 16 member ensemble forced with Hadley Centre SSTs. The 100
156 ensemble members are initialized on December 1 2013 with different initial conditions
157 taken from December 1 atmospheric and land surface states of long model simulations
158 with repeating climatological Hadley SSTs.
- 159 ii. 100 member ensembles simulating the 100 days beginning December 1 in which fixed
160 idealized SST anomalies are added to the Hadley Centre SST climatology. An ad-
161 ditional 100 member ensemble was generated using the same atmosphere and land
162 initial conditions but climatological SSTs. The ensemble means of the daily differ-
163 ences between the 100 perturbed and control pairs were then analyzed. The perturbed
164 simulations are forced by “box-SST anomalies” centered on the Equator at different
165 longitudes from the Indian Ocean to the eastern tropical Pacific. Each anomaly has
166 a maximum of $1^{\circ}C$ and is in a box centered on the Equator stretching from $10^{\circ}S$ to
167 $10^{\circ}N$ and spanning 30° in longitude. One pass of a 1-2-1 smoother in space was ap-
168 plied to the anomalies to remove the sharp SST anomaly gradients at the box edges.

169 Experiments were run for both warm and cold SST anomalies with results shown for
170 the warm minus cold experiments divided by two.

171 **3. Atmosphere-ocean conditions during winter 2013/14**

172 We focus on the winter of 2013/14 which was the driest, as measured by all-California,
173 November through April precipitation reduction, so far in the current California drought
174 (Seager et al. 2015). We also focus on the December through February (DJF) season at the
175 heart of winter.

176 *a. Observed and Reanalysis SST, surface flux, precipitation and circulation anomalies*

177 Figure 1 shows the observed 200mb height and precipitation anomalies from the NCEP-
178 NCAR and ERA-Interim Reanalyses, the GPCP and CPC CMAP precipitation anomalies,
179 the ERSSTv4 SST anomaly, and the latent plus sensible OA flux anomaly for DJF 2013/14.
180 The height anomaly, which is very similar for both Reanalyses, includes a north-northwest to
181 south-southeast oriented ridge immediately west of the North American coast and extending
182 from Alaska to Mexico. The ridge is part of a more general area of high geopotential heights
183 that extends west over the North Pacific, Bering Sea and eastern Siberia. There was also
184 a deep trough centered over Hudson Bay, responsible for the very cold winter in northeast
185 North America (Hartmann 2015; Baxter and Nigam 2015), low heights over the mid-latitude
186 North Atlantic and high heights over the subtropical North Atlantic (although not with the
187 canonical positive North Atlantic Oscillation pattern).

188 The precipitation anomaly associated with this height pattern shows the dry conditions
189 along the U.S. west coast and expanding into British Columbia, northwest Mexico and the
190 central U.S. The west coast and central North America dry anomalies are under northerly
191 upper level flow. Over the North Pacific, wet anomalies occur on the western, southerly,
192 flowing flank of the ridge and another dry anomaly under northerly flow over the northwest
193 Pacific. In the tropics there was a dry anomaly over the central to eastern Pacific, a wet
194 anomaly northwest of Papua New Guinea, generally neutral to dry conditions over the mar-

195 itime continent and wet conditions over the west-central Indian Ocean. These features are
196 common across the four precipitation estimates but there are some notable differences in
197 the amplitude and pattern between the datasets. For example NCEP-NCAR has a more co-
198 herent west Pacific-maritime continent wet anomaly but not the wet Indian Ocean anomaly
199 seen in the other three estimates.

200 In the reanalysis-based moisture budget analysis of Seager et al. (2014b), precipitation
201 at the west coast of North America arises from westerly winds, orographic uplift at the
202 coast and the propagation onshore from the west of storm systems within the Pacific storm
203 track. Further, Seager et al. (2014b) also show that interannual variability of the moisture
204 convergence by transient eddies is very important, especially for producing precipitation in
205 southern California and northern Mexico in winter. The west coast ridge of winter 2013/14
206 and the associated lack of storm systems impinging on the west coast of the U.S. was re-
207 sponsible for the dry conditions. A measure of the storm track activity is the high-pass
208 filtered upper tropospheric meridional velocity variance. Using daily data from the NCEP
209 Reanalysis we computed this using a fourth order Butterworth filter with a 10 day cutoff and
210 the middle right panel of Figure 1 shows the anomaly for DJF 2013/14. There was a rather
211 striking banded structure across the eastern North Pacific and North America with reduced
212 eddy activity centered around the latitude of California and increased activity to the north.
213 This implies fewer and/or weaker storms entering the southern portions of the west coast
214 and, along with the mean high pressure ridge, is consistent with reduced precipitation (and
215 the California drought).

216 The SST anomaly during DJF 2013/14 (contours in the middle left panel of Figure 1,
217 colors in Figure 2) shows cool anomalies in the central to eastern tropical Pacific, warm
218 anomalies in the western tropical Pacific, a broad region of warm anomalies in the Indian
219 Ocean south of the Equator¹ and a remarkably warm anomaly in the northeast Pacific south
220 of Alaska and west of British Columbia and Washington State. The colors in the middle left
221 panel of Figure 1 are the surface latent plus sensible heat flux, defined here as positive into
222 the ocean. Notably the warm North Pacific SST anomalies are associated with anomalous

¹The Indian Ocean warm SST anomalies strengthen to the south of the domain shown but were not associated with increased precipitation that would force an atmospheric response.

223 flux of heat into the ocean, i.e. atmospheric forcing of the anomalies. Further, Bond et al.
224 (2015) performed an ocean mixed layer heat budget analysis of the northeast Pacific warm
225 anomaly and found the prime driver of it was a reduction in entrainment of cool water into
226 the mixed layer as a consequence of extreme low wind speeds. Hence, via both surface fluxes
227 and mixed layer processes, the northeast Pacific warm anomaly appears as a result of the
228 west coast ridge and not a driver. In contrast, the warm SST anomaly in the tropical west
229 Pacific was associated with an anomalous flux of latent plus sensible heat from the ocean to
230 the atmosphere. There is also a region on the Equator at the dateline of anomalous ocean
231 heat uptake. This corresponds to a region of negative precipitation anomaly in the GPCP
232 data but is at the border between positive and negative SST anomalies in the ERSSTv4
233 analysis.

234 These associations are suggestive of ocean driving of the atmosphere in the tropical
235 west Pacific and the opposite over the North Pacific, an entirely familiar state of affairs in
236 interannual climate variability that has been well known dating back to Alexander (1992a,b),
237 Cayan (1992) and Lau and Nath (1994, 1996). However, it should be noted that what the
238 SST anomaly was during DJF 2013/14 is not clear. Figure 2 (left column) shows maps for
239 the anomaly, all relative to the same 1979 to 2014 climatology, for the Hadley, ORAS4 and
240 ERSSTv4 data sets. All three disagree on the amplitudes of the warm SST anomalies in the
241 North Pacific (by about $0.5K$) and in the tropical west Pacific and the cold anomaly in the
242 central equatorial Pacific Ocean (typically by less than $0.5K$). Some of this disagreement is
243 to be expected since the ERSSTv4 data set only uses in situ measurements while Hadley and
244 ORAS4 also use satellite data (but with different sources) and the analysis methods used to
245 obtain gridded data sets differ.

246 *b. Atmosphere model response to observed estimates of SST anomalies*

247 The differences in the SST anomalies matter for the atmospheric response. Figure 2 shows
248 the modeled ensemble mean 200mb height and precipitation response to the DJF 2013/14
249 global SST anomalies when the Hadley, ORAS4 and ERSSTv4 anomalies are added to the
250 Hadley climatological SST for CCM3 (middle column) and CAM5.3 (right column). Five of

251 the six combinations of SST forcing and model have high height anomalies near or at the
252 west coast, with CAM5.3 and Hadley SST forcing the exception. The elongated northwest to
253 southeast orientation of the ridge is most realistic with the ORAS4 SST forcing. The Hudson
254 Bay trough is only produced with ORAS4 SST forcing within CCM3. The height anomalies
255 are, as expected considerably smaller than observed, consistent with SST-forcing only being
256 partially responsible for the ridge. The associated precipitation anomalies also largely agree
257 with the observations with dry across the central to eastern tropical Pacific, wet over the
258 western tropical Pacific. However, with Hadley SST forcing in particular, the western tropical
259 Pacific wet anomaly is split in two by a westward extension of the equatorial Pacific dry zone.
260 The models also have unrealistic dry anomalies over the Maritime Continent. The model
261 simulations all agree on wet conditions over the southern Indian Ocean and dry to the north
262 which is clearly a simple response to the warm-cold south-north Indian Ocean SST anomalies
263 but which is only hinted at in the GPCP observed precipitation anomaly. The responses in
264 heights and precipitation of the two atmosphere models are quite similar and both models
265 show the sensitivity to choice of SST forcing dataset.

266 Despite the noted aspects of model-observations agreement all three forced responses dif-
267 fer. This is despite the experiments being done with the same model and with the anomalies
268 being imposed on the same SST climatology and the ensemble containing 100 members which
269 effectively isolates the forced response. The differences between the responses to the three
270 SST anomaly estimates appearing in each atmosphere model indicates that the differences
271 in SST anomalies matter and, of course, we cannot tell easily which SST data set is more
272 accurate. It is sobering to realize that, in this important case, modern observations and
273 analysis methods cannot constrain SST anomalies to the accuracy required to successfully
274 model the atmospheric response.

275 An additional problem with SST-forced experiments for winter 2013/14 concerns the
276 North Pacific warm SST anomaly. In experiments we have performed with SST forcing
277 restricted to the tropics only and the North Pacific only, it is clear that the response to
278 global SSTs seen in Figure 2 involves both. However, when the North Pacific SST anomaly
279 is imposed alone the atmosphere model responds by increased ocean to atmosphere surface
280 heat flux, northerly winds above (which can balance the heating with advective cooling as in

281 Hoskins and Karoly (1981)) and a high to the west. This response is essentially the opposite
282 of the flow-flux relationship seen in observations during DJF 2013/14 (Figure 1 and (Bond
283 et al. 2015)) and is consistent with being a spurious model response to an imposed SST
284 anomaly that was in fact generated by the atmospheric flow pattern. All of the simulated
285 responses in Figure 2 will be corrupted by some element of this spurious response.

286 *c. On the difference in amplitude of observed and modeled circulation anomalies*

287 In addition to being different from one another all the model circulation responses are
288 much weaker than the observations. We found that the observed west coast ridge height
289 anomaly is about one and a half times the standard deviation of the DJF seasonal mean
290 height anomalies. In contrast the modeled ensemble mean 60 day average height anomaly at
291 the west coast is only about half of the standard deviation of 60 day mean height anomalies
292 across the 100 member ensemble. These relative values are consistent with Seager et al.
293 (2015) suggestion that only about a third of the circulation anomaly could be explained in
294 terms of SST-forcing leaving the rest to be explained by internal atmospheric variability. The
295 relatively small SST-forced signal to atmospheric noise ratio means that a large ensemble
296 (e.g. 100 members) is required to capture the response in the ensemble mean.

297 **4. Constructive modeling of the west coast ridge of win-** 298 **ter 2013/14**

299 The above results and arguments make clear that we cannot expect to explain the ori-
300 gin of the circulation anomalies of DJF 2013/14 by simply imposing an “observed” SST
301 anomaly as the lower boundary condition for an atmosphere model. Instead we will adopt a
302 more roundabout route that seeks to identify a combination of idealized SST and associated
303 diabatic heating anomalies that can reproduce the circulation anomaly.

304 *a. “Box-SST anomaly” experiments*

305 Turning to the results of the “box-SST anomaly” modeling experiments, we begin by
306 noting that the circulation of DJF 2013/14 is unlike any familiar wave trains produced
307 by these localized SST anomalies. Figure 3 shows the 200mb geopotential height anomaly
308 responses (right column) to the imposed box SST anomalies (left column). A warm SST
309 anomaly in the central equatorial Pacific Ocean (fourth row) forces a single wave train that
310 is quite characteristic of El Niño events with a low height anomaly over the North Pacific
311 and a high anomaly centered over western Canada. The same size SST anomaly to the east
312 (bottom) is less effective at forcing a response in the height field. As the warm anomaly is
313 moved west the response moves west too but also weakens and then changes character when
314 the warm SST box is placed in the Indian Ocean. In that case (top panel) a rather zonally
315 symmetric response results with low height anomalies over northern Canada and high height
316 anomalies over the North Pacific and North Atlantic, somewhat reminiscent of the warm
317 Indian Ocean-positive North Atlantic Oscillation connection identified by Hoerling et al.
318 (2001). The observed DJF 2013/14 height anomaly is not very akin to any of these patterns,
319 or their opposite, but instead is more akin to some combination of these anomalies indicating
320 that SST anomalies across the Indo-Pacific Ocean may have collectively contributed to the
321 circulation anomaly.

322 *b. Optimal combinations of “box-SST anomaly” responses that match DJF 2013/14*

323 Given that the circulation of DJF 2013/14 cannot be easily explained as a response to a
324 single localized SST anomaly, can it be explained as a combination of wave responses to a
325 variety of SST anomalies and, if so, can this be understood in terms of linear superposition
326 of the different waves? To assess this we seek the optimal linear combination of “box-SST
327 anomaly” response patterns that best matches the observed DJF 2013/14 200mb height
328 anomaly for all longitudes and from $25^{\circ}N$ to $75^{\circ}N$. This map, Z'_{NCEP} , is our target pattern
329 and is a subset of the field shown in Figure 1.

330 We denote the 200mb heights from the box-SST anomaly experiments as Z_j . We use a
331 constrained linear least squares optimization to find the best approximation of the Z'_{NCEP}

332 using linear combinations of the Z'_j with the realistic constraint that the SST anomalies are
 333 less than $0.6K$. This can be expressed as the problem of finding N constants, c_j , which
 334 achieve the distance minimization:

$$\min_{\mathbf{c}} \left(\left\| \sum_{j=1}^N c_j Z'_j(\mathbf{x}) - Z'_{NCEP}(\mathbf{x}) \right\| \right) \quad (1)$$

335
 336 subject to the constraint:

$$|c_j| \leq 0.6, \quad (2)$$

337 where the global area-weighted energy norm over all gridpoints $\mathbf{x} = (\lambda, \phi)$, where λ is
 338 longitude and ϕ is latitude, is

$$\|f(\mathbf{x})\|^2 \equiv \frac{\sum_{\mathbf{x}} f^2(\mathbf{x}) \cos(\phi)}{\sum_{\mathbf{x}} \cos(\phi)}.$$

339 Finding the c_j for $j = 1$ to 5 from the above procedure produces the 200mb height
 340 anomaly pattern shown in Figure 4. The optimization is able to create a west coast-North
 341 Pacific ridge and also a weak Hudson Bay trough pattern that, though far from a perfect
 342 match, has clear similarities to that observed although much weaker. The differences in
 343 structure (including the ridge not extending far enough south) and amplitude support the
 344 idea that the observed pattern combines an SST-forced response with constructive internal
 345 atmosphere variability. Agreement between observed and modeled height anomalies is poor
 346 over Asia and the North Atlantic perhaps indicating an even greater role there for internal
 347 atmospheric variability in explaining the observed pattern. Figure 4 also shows the cor-
 348 responding SST and precipitation anomalies, derived from the same linear combination of
 349 “box-SST anomaly” experiments. The optimal circulation anomaly arose as a response to a
 350 collection of SST anomalies and associated precipitation anomalies. The best match to ob-
 351 servations requires a modestly warm eastern Indian Ocean, near normal over the Maritime
 352 Continent region, warm in the western tropical Pacific Ocean and cool across the central
 353 and eastern tropical Pacific Ocean. The precipitation anomalies the model produces closely
 354 match the SST anomalies in a warm-wet, cool-dry sense as expected, and also have some
 355 similarity to the observed precipitation anomalies in Figure 1 though the Indian Ocean wet
 356 anomalies appear too large. It is noteworthy that, out of all the possible combinations of

357 sign and amplitude and location of SST anomalies that the optimization could have chosen
358 to find a response field that best matches the observed height field, it chose one that has a
359 clear resemblance to reality.

360 *c. Checking for linearity of the response to collections of SST anomalies*

361 Identifying a linear combination of “box-SST anomaly” responses that best matches the
362 observed circulation does not mean that, if forced with the associated linear combination
363 of SST anomalies, the atmosphere model would reproduce the same circulation. This is
364 because the model is nonlinear and allows for the possibility that the waves forced from
365 the various ocean regions will interact with each other to produce a response that departs
366 from the linear assumption. To check this we forced the atmosphere model with the optimal
367 linear combination SST pattern and the results are shown in the lower panel of Figure 4.
368 The model 200mb height response to the optimized SST anomalies is quite similar in the
369 important details to the optimal sum of the individual box experiments, confirming the
370 basic linearity of the response. That is, the total response can be understood as the linear
371 combination of waves forced by the components of the total SST anomaly field with little
372 important interaction between the forced waves.

373 **5. Tropical Indo-Pacific SST anomaly forcing of circula-**
374 **tion and storm track anomalies in the eastern North**
375 **Pacific and North America sector**

376 Tropical SST anomalies can exert a strong influence on the strength and latitude of the
377 Pacific storm track over the eastern North Pacific and west coast of North America. Return-
378 ing to the “box-SST anomaly” experiments, Figure 5 shows the ensemble mean change in
379 the 200mb high pass filtered meridional velocity variance averaged over days 40-100 of each
380 experiment. Depending on where the SST anomaly is located it can have quite different
381 effects on the Pacific storm track. For a warm SST anomaly in the central equatorial Pacific

382 a rather classic El Niño-like southward displacement and strengthening of the storm track
383 from the central North Pacific to North America occurs as analyzed in detail in Seager
384 et al. (2010b) and Harnik et al. (2010). The argument in those papers is that the storm
385 track displacement occurs as the transient eddies are refracted more equatorward as a conse-
386 quence of strengthened subtropical westerly winds that occur poleward of the diabatic deep
387 convective heating anomaly generated by the warm SST anomaly. A warm SST anomaly
388 in the far western tropical Pacific generates a similar but weaker southward storm track
389 displacement. In contrast, a warm SST anomaly in the maritime continent region induces
390 only a weak response while one over the Indian Ocean causes a strong poleward displacement
391 with increased eddy activity over British Columbia and Alaska and decreased activity over
392 California and Mexico.

393 Returning to Figure 1 (middle right panel), it is seen that winter 2013/14 had a reduction
394 of eddy activity centered over the eastern North Pacific and North America at the latitude of
395 California with increased activity over southwestern Canada and over the subtropical eastern
396 North Pacific. From Figure 5, this would appear to be a pattern that could be induced by a
397 combination of tropical SST anomalies, including a warm anomaly over the western tropical
398 Pacific, which can cause a reduction of eddy activity at the location of California and an
399 increase over the subtropical North Pacific Ocean to the south of California.

400 Figure 6 shows the evolution of the mean and transient circulation response in the model
401 forced by the switch-on of the optimized SST anomaly pattern. Here the ensemble mean
402 anomaly will, over the 10-15 day time period of initial value predictability when the ensemble
403 members closely resemble each other, represent the daily evolution of the forced response
404 to the imposed SST anomaly and hence we show daily values. After that, the ensemble
405 members will diverge and we show time averaged quantities to identify more closely the
406 SST-forced response. The initial response involves positive height anomalies straddling the
407 equator over the west Pacific Ocean and negative height anomalies straddling the central
408 Pacific Ocean: classic Gill (1980) responses to convection and vertical motion anomalies
409 above warm and cool SST anomalies. By day 8 these responses are already establishing
410 the west coast ridge. A weaker response to Indian Ocean SST anomalies is also apparent.
411 The wave trains lead to intensification of the west coast ridge over the subsequent week. In

412 tandem with the wave trains, the weaker eddy activity over the midlatitude eastern North
 413 Pacific Ocean and the United States and Mexico begins to be established by day 8 and also
 414 intensifies with the height anomalies over the subsequent week. The eddy weakening occurs
 415 where there are local easterly anomalies at 200mb (deduced from the height anomalies) and
 416 the strengthening where anomalies are westward. This relation is consistent with changes in
 417 transient eddy propagation paths responding to the changes in the mean flow as in Seager
 418 et al. (2010b) and is qualitatively similar to that observed (Figure 1).

419 **6. The dynamical balance within the mean and tran-** 420 **sient circulation anomalies of winter 2013/14**

421 *a. The quasi-equilibrium vorticity balance in Reanalysis and model simulation*

422 How did the atmosphere achieve a seasonal mean state during winter 2013/14 that in-
 423 cluded such strong departures from the normal state? To examine this we turn to the upper
 424 troposphere monthly mean vorticity budget which can be written as:

$$\frac{\partial \hat{\zeta}}{\partial t} + \hat{\mathbf{u}} \cdot \nabla \hat{\zeta} + \beta \hat{v} = -(\hat{\zeta} + f) \nabla \cdot \hat{\mathbf{u}} - \nabla \cdot (\widehat{\mathbf{u}'' \zeta''}) + \hat{F}, \quad (3)$$

425 where the hats denote monthly means and the double primes departures therefrom, ζ is
 426 relative vorticity, \mathbf{u} is the horizontal vector velocity, f is the Coriolis parameter and β its
 427 meridional gradient, v is meridional velocity, F includes friction, diffusion and the residual
 428 imbalance and t is time. Terms involving vertical advection of vorticity, which tend to be
 429 small, have been neglected.

430 A common way to diagnose forcing of Rossby waves by tropical heating anomalies is
 431 to separate the anomalous flow into its rotational, denoted by subscript ψ , and divergent,
 432 denoted by subscript χ , components, i.e. $\hat{\mathbf{u}} = \hat{\mathbf{u}}_\psi + \hat{\mathbf{u}}_\chi$. Using this, and denoting anomalies
 433 by a single prime and climatological values by an overbar, e.g. $\hat{u} = \hat{u}' + \overline{\hat{u}}$, the anomaly
 434 vorticity equation can be rewritten as:

$$\frac{\partial \hat{\zeta}'}{\partial t} + \hat{\mathbf{u}}'_\psi \cdot \nabla \hat{\zeta}' + (\hat{\mathbf{u}}'_\psi \cdot \nabla \hat{\zeta}' + \beta \hat{v}'_\psi) = -(\hat{\zeta}' + f) \nabla \cdot \hat{\mathbf{u}}'_\chi - \hat{\zeta}' \nabla \cdot \hat{\mathbf{u}}_\chi - \beta \hat{v}'_\chi - \hat{\mathbf{u}}_\chi \cdot \nabla \hat{\zeta}' - \hat{\mathbf{u}}'_\chi \cdot \nabla \hat{\zeta}' - \nabla \cdot (\widehat{\mathbf{u}'' \zeta''})' + \hat{F}'. \quad (4)$$

435 These terms were computed for the observations from the NCEP-NCAR and ERA-Interim
 436 Reanalysis averaged over DJF 2013/14 with anomalies defined as relative to a January 1979
 437 to April 2014 climatology. The results for both Reanalyses were found to be very similar
 438 and here we show just the results from NCEP-NCAR since these were obtained at a spatial
 439 resolution more akin to that of the model simulations. The right hand side, minus the
 440 damping term, is referred to as the Rossby Wave Source (RWS) (Sardeshmukh and Hoskins
 441 (1988); Trenberth et al. (1998) who use somewhat different notation). Watson et al. (2016)
 442 show the RWS from the ERA-Interim analysis for the west Pacific domain and separate
 443 it into divergent and advection terms and their results are very similar to those shown
 444 here from NCEP-NCAR but we continue by breaking the term down into its constituent
 445 parts to afford a more detailed process understanding. It was found that $\partial\hat{\zeta}'/\partial t$, $\hat{\zeta}'\nabla\cdot\hat{\mathbf{u}}_\chi$,
 446 $\hat{\mathbf{u}}_\chi\cdot\nabla\hat{\zeta}'$ were sufficiently smaller than the other terms so that they could be neglected in
 447 understanding the vorticity balances and its establishment. $\hat{\mathbf{u}}'_\chi\cdot\nabla\hat{\zeta}$ is also small but is
 448 retained since this term has been appealed to as an important forcing in prior literature.
 449 Written in this way the rotational flow, as described by the left hand side, can be understood
 450 as a response to forcing involving the divergent flow on the right hand side. The planetary
 451 vorticity advection and the advection of anomalous vorticity by the mean flow extensively
 452 balance each other as expected within a stationary barotropic Rossby wave and are grouped
 453 together $\left(\hat{\mathbf{u}}_\psi\cdot\nabla\hat{\zeta}'+\beta\hat{v}'_\psi\right)$ to allow better seeing the smaller imbalance that allows vertical
 454 motion. The six larger remaining terms from Eq. 4 are shown in Figure 7.

455 The vorticity balance anomalies are seen to occur as part of waves of anomalies that
 456 stretch to North America from the Indian and tropical Pacific Ocean regions. Across the
 457 east Pacific and North America there is a balancing relationship between, on the one hand,
 458 the sum of mean flow advection of the vorticity anomalies and advection of the planetary
 459 vorticity by the rotational meridional wind anomaly $\left(\hat{\mathbf{u}}_\psi\cdot\nabla\hat{\zeta}'+\beta\hat{v}'_\psi\right)$, panel b) and, on the
 460 other hand, upper tropospheric convergence and vortex compression $-(\hat{\zeta}+f)\nabla\cdot\hat{\mathbf{u}}'_\chi$, panel
 461 e). The upper troposphere convergence induces subsidence (not shown) at the west coast
 462 of North America which would suppress precipitation, consistent with drought conditions.
 463 In contrast to the balance over the eastern Pacific-North America sector, over the Indian
 464 and west Pacific sectors, the advection of the mean relative vorticity by the rotational flow

465 anomalies (panel a), dominated by $\hat{v}'\partial\hat{\zeta}/\partial y$, is important. This term sets up an east-west
466 varying pattern that reflects the zonal variation in meridional flow anomalies that arises
467 from the circulation responses to the multiple SST and convection anomalies in the tropics.
468 These flow anomalies are located in a region of strong zonally uniform meridional gradient
469 of mean relative vorticity (not shown) giving rise to this complex pattern.

470 The mechanism of establishment of the forcing for the Rossby waves differs somewhat
471 from classical thinking (Sardeshmukh and Hoskins 1988; Trenberth et al. 1998) in that,
472 across Asia and the subtropical west Pacific, the advection of mean relative vorticity by the
473 anomalous divergent flow is much smaller than that by the rotational flow. Hence we do
474 not have a clean separation with the rotational flow evolving in response to changes in the
475 divergent flow. Instead the forced rotational flow interacts with the mean flow to cause a
476 further evolution of the rotational flow anomaly.

477 The vorticity budget terms were also averaged over the last 60 days of the optimal SST-
478 forcing simulations. Anomalies in this case are the difference between the SST-perturbed and
479 unperturbed ensemble means. It was found that the terms that were small in the Reanalysis
480 were also small in the model and the same six larger terms in the model are shown in Figure
481 8. The relative importance of the terms in the vorticity budget are very similar between the
482 models and the Reanalysis. The one exception is the much smoother transient eddy vorticity
483 convergence in the model than the Reanalysis which simply comes about from the averaging
484 across a 100 member ensemble compared to Nature's single realization. The individual terms
485 in the vorticity balance also bear some similarity between model and Reanalysis. Over
486 western North America the model agrees with the observations that the upper troposphere
487 convergence and, hence, subsidence below, arises from a three way balance between vortex
488 stretching, advection of planetary vorticity by the rotational meridional velocity anomaly
489 and advection by the mean flow of the vorticity anomaly (panel b). The model agrees that
490 advection of the mean relative vorticity by the rotational flow (panel a) dominates over
491 that by the divergent flow (panel c). Similarly this sets up in the model a zonally varying,
492 meridionally confined, anomalous vorticity tendency over south Asia and the subtropical
493 west Pacific. The locations of the features within this term, however, do not agree between
494 the model and Reanalysis, which could be due to model bias in the location of the tropical

495 heating, the flow response, or in the mean state which allows a phase error in the wave
496 response.

497 The transient eddy vorticity flux convergence term (panel f) is not small. However it
498 also does not appear to systematically contribute to the maintenance of the large scale
499 circulation anomaly pattern being instead rather noisy. This is in contrast to the results
500 of Seager et al. (2003, 2010b) and Harnik et al. (2010) who found that transient eddy
501 momentum fluxes were important to developing and sustaining mean flow anomalies during
502 El Niño events. However the results are not necessarily inconsistent. The earlier results
503 concerned El Niño events which could have a different eddy-mean flow interaction process
504 to that occurring during winter 2013/14 and its model analog. Also the earlier results made
505 much of the case for a positive eddy-mean flow feedback by analyzing longitudinally averaged
506 quantities whereas here our focus is on explaining the west coast ridge of winter 2013/14, a
507 very longitudinally localized feature.

508 *b. Observed and modeled tropical forcing of circulation anomalies*

509 Copsey et al. (2006) point out that imposing SST anomalies over the Indian Ocean can
510 lead in a model to wrong sign precipitation and surface pressure responses. An incorrect
511 response would also be apparent in the divergent wind response to the SST and precipitation
512 anomalies. Since our arguments to date rely heavily on an SST-forced model, and the optimal
513 SST methodology allows this error to occur, in Figure 9 we show the DJF 2013/14 anomalies
514 of surface pressure over the ocean and 200mb divergent wind and velocity potential (Φ' ,
515 related as $\hat{\mathbf{u}}'_\chi = \nabla \hat{\Phi}'$) from NCEP Reanalysis and averaged over the last 60 days of the
516 model simulations of the response to the optimal SST pattern. The upper troposphere
517 divergence anomalies over the western tropical Pacific are striking in both observations and
518 model. The model has a weaker divergence center over the Indian Ocean, and a convergence
519 center over southeast Asia, that are barely present in observations. The model correctly
520 reproduces the low surface pressure anomaly across the Indian Ocean and western tropical
521 Pacific and high anomalies in the central (observations) and eastern (model) tropical Pacific.
522 The comparison suggests the model response is more realistic over the Pacific sector of the

523 tropics than the Indian Ocean sector. This is reassuring as the optimization invokes SST
 524 anomalies that are greater over the Pacific than the Indian Oceans. Further much of the wave
 525 forcing is by the rotational as opposed to divergent flow, although these components will
 526 be related. However, this comparison provides some additional confidence that the model
 527 results inform on the potential role of the tropical SST anomalies in generating the west
 528 coast ridge of winter 2013/14. (Agreement is poor over the Atlantic consistent with little
 529 evidence that circulation anomalies there were forced from the Indian and Pacific Oceans.)

530 *c. The transient evolution of the vorticity balance in the model simulation*

531 It is not possible to establish cause and effect in the establishment of the vorticity balance
 532 in the Reanalysis because the atmosphere is always in a statistical equilibrium with the slowly
 533 evolving SST anomalies. As in Figure 6 for the height field and storm track, here we examine
 534 how the vorticity budget evolves on a day-by-day and weekly basis. Results are shown in
 535 Figure 10 for the leading terms in the vorticity budget given by:

$$\mathbf{u}'_{\psi} \cdot \nabla \bar{\zeta} + \bar{\mathbf{u}}_{\psi} \cdot \nabla \zeta' + \beta v'_{\psi} = -f \nabla \cdot \mathbf{u}'_{\chi}. \quad (5)$$

536 Here the anomalies and climatology are both on the daily timescale with the anomalies
 537 defined as the difference between the SST-perturbed and control ensemble means. Early on
 538 at day 5 there are various vorticity tendency terms related to the advection of the mean
 539 relative vorticity gradient by the anomalous rotational flow across the tropical Pacific north
 540 of the Equator. This term is dominated by its meridional component $\hat{v}'_{\psi} \hat{\zeta}'_y$ component (not
 541 shown). This entire term has grown by day 11 and is being balanced in large part by the
 542 sum of mean flow advection of the relative vorticity anomaly and the anomalous advection
 543 of planetary vorticity and to a lesser extent by the term involving the upper troposphere
 544 divergence anomaly. The latter convergence over the west coast of North America that, by
 545 mass continuity, will require subsidence below, is only barely evident by day 17 but intensifies
 546 over subsequent weeks. Further examination shows that, over the west Pacific, the advection
 547 of mean relative vorticity by the anomalous rotational flow is dominated by the meridional
 548 flow anomaly but in the east Pacific-North America sector the advection by anomalous zonal
 549 flow is the leading term. The vorticity balance terms intensify to day 17 but the balance

550 among the terms remains essentially the same.

551 This can be understood in terms of the transient evolution of the flow anomaly field
552 $(\hat{u}'_{\psi}, \hat{u}'_{\chi}, \hat{v}'_{\psi}, \hat{v}'_{\chi})$ as shown in Figure 11. The warm SST and positive precipitation anomaly over
553 the west Pacific Ocean excites local upper troposphere off-equatorial anticyclonic anomalies
554 to the west and equatorial westerly and cyclonic anomalies to the east. The latter are more
555 clear because the heating forced response to the west is in a location where there will also
556 be responses to the SST anomalies over the Maritime Continent region and Indian Ocean.
557 Looking at the transition from day 5 to day 11, the cyclonic anomaly over the east Pacific
558 is now at the root of a wave train that has propagated northeastward and placed easterly
559 anomalies at the west coasts of the United States and Mexico. In addition a wave easily seen
560 in the meridional flow field has propagated from the northern Indian-south Asia-tropical west
561 Pacific region eastward across the Pacific and placed northerly flow at the west coast centered
562 on the Canada-U.S. border region. The vorticity balance that is established therefore arises
563 from a combination of these wave fields originating across the Indo-Pacific region but with
564 the end result of high pressure and subsidence at the west coast of North America that would
565 act to suppress precipitation.

566 **7. Explaining the west coast ridge of winter 2013/14** 567 **in terms of SST-forcing plus internal atmospheric** 568 **variability**

569 The modeling results presented, and those by others (e.g. Watson et al. (2016)), do
570 not support the idea that the full amplitude of the west coast ridge of winter 2013/14 was
571 SST-forced. Instead it is argued that the full amplitude is explained by a combination of a
572 SST-forced response and internal atmospheric variability acting constructively. Given that
573 we have ensembles with 100 members which can span a wide, if not complete, range of in-
574 ternal atmosphere variability, it is worth examining if some ensemble members have a ridge
575 amplitude as large as that observed. To determine this we computed the pattern correla-
576 tion between the observed DJF 2013/14 200mb height anomaly and that of the ensemble

577 members in the simulation forced by the optimal SST pattern, with the anomaly defined
578 as the difference between the ensemble member and the 100-member mean of the control
579 ensemble with unperturbed SSTs. Figure 12 plots the height and precipitation anomalies
580 of the four ensemble members with the highest correlation. It is possible to get a height
581 anomaly very similar in pattern (including the Hudson Bay trough) and magnitude to that
582 observed. Notably these ensemble members also had tropical precipitation anomalies akin
583 to the ensemble mean and the observations. We also performed the same calculation using
584 the 100 control ensemble members with anomalies defined as relative to the ensemble mean
585 and found that, even without anomalous SST forcing, some ensemble members could pro-
586 duce a west coast ridge akin in pattern and magnitude to that observed. Figure 12 also,
587 therefore, shows histograms of the pattern correlations for the two 100 member ensembles.
588 While both ensembles essentially span -1 to 1, the SST-forced ensemble, relative to the un-
589 perturbed ensemble, is clearly shifted towards more positive values. The two distributions
590 are significantly different, according to the Kolmogorov-Smirnov test, with greater than 99%
591 confidence. This result illustrates how internal atmospheric variability could alone create
592 height anomalies akin to the one observed but that the presence of the Indo-Pacific SST
593 anomalies made the observed height anomaly considerably more probable. For example,
594 the presence of the SST-forcing made anomalies that matched the observed with a pattern
595 correlation of 0.6 or more three times more likely than without the SST anomalies.

596 8. Conclusions and Discussion

597 We have investigated the dynamical causes of the North American west coast ridge of
598 winter 2013/14 that caused the driest winter during the recent California drought and ex-
599 amined the role in generating it of SST anomalies in the tropical Pacific and Indian Oceans.
600 Conclusions are as follows:

- 601 • Prior work has suggested the drought-inducing North American west coast ridge of
602 winter 2013/14 was partly forced by SST anomalies. However different SST data sets
603 disagree on the amplitude and to some extent the pattern of the SST anomalies with the
604 result that the same atmosphere model forced by the different SST data sets simulates

605 the ridge with different levels of realism.

- 606 • Motivated by the uncertainty in regard to the SST anomalies that were actually present
607 in winter 2013/14, we adopted a “constructive modeling” approach and found an op-
608 timal pattern of tropical Indo-Pacific SST anomalies that produced a model response
609 that best matched the observed Northern Hemisphere height anomaly in DJF 2013/14.
610 A pattern with a warm SST anomaly in the west Pacific, cool in the central Pacific,
611 near neutral in the Maritime Continent region and weak warm in the Indian Ocean
612 produces a height response that provides the best match including a west coast ridge.
613 The height response can be understood as a linear combination of waves forced by
614 the individual anomalies. Despite the optimization methodology, the modeled ridge is
615 considerably weaker than that observed lending support to the idea that SST-forcing
616 played a limited, if important, role in generating the ridge.

- 617 • In both observations for DJF 2013/14 and the optimal forcing simulations the west
618 coast ridge is also associated with suppression of storm track activity with increased
619 activity towards the north and south. This rearrangement of transient eddy activity,
620 which essentially acts to shield California from moisture-laden storms, would have
621 aided in generating drought conditions.

- 622 • The fundamental features of the vorticity balance within the circulation anomaly are
623 associated with the mean flow terms involving advection of the mean relative vorticity
624 field by the rotational flow, advection of the relative vorticity anomaly by the mean
625 zonal flow, the anomalous planetary vorticity advection and vortex stretching. It is
626 vortex compression over the west coast that will act to induce subsidence and also
627 suppress precipitation. We do not find clear evidence of a feedback between the eddy
628 vorticity fluxes and the mean flow.

- 629 • The transient day-by-day and week-by-week evolution of the model response to the op-
630 timal SST forcing shows that the collection of tropical SST anomalies generate upper
631 troposphere rotational flow anomalies that create anomalous advection of mean rela-
632 tive and planetary vorticity and force Rossby waves that propagate and within days

633 reach the west coast of North America establishing the ridge by the vorticity balance
634 described above. As the mean flow circulation anomaly develops so does the reduction
635 in eddy activity over the west Pacific and North America at the latitude of the United
636 States and Mexico.

- 637 • A combination of SST-forced response and internal atmosphere variability can provide
638 a reasonable match to the observed height anomaly in terms of pattern and amplitude.
639 The presence of SST forcing notably increases the probability of such a height anomaly
640 occurring.

641 To conclude, the work presented here is highly suggestive that tropical Indo-Pacific SST
642 anomalies and associated precipitation anomalies forced a collection of Rossby wave responses
643 that in sum contributed to the unusual North American west coast ridge of winter 2013/14.
644 Hence, we argue, that the ridge depended on a more general anomalous tropical ocean state
645 than just the warm western tropical Pacific whose impacts were focused on by Watson et al.
646 (2016). The results are, however, not conclusive largely because the actual SST anomalies
647 during this winter are not known to the level of accuracy that is apparently needed to suc-
648 cessfully reproduce in models the correct atmospheric response. Hence it remains uncertain
649 exactly what SST anomalies were responsible and also whether there was an additional role
650 in the wave forcing for precipitation anomalies that were not tied to the underlying SSTs.
651 A clear avenue for future research must be to determine why different state-of-the-art SST
652 data sets differ to the degree they do in the modern era of quite abundant observational
653 data. A second avenue for research should be to determine what caused the drought-forcing
654 SST anomalies and how well they, and the atmospheric response to them, can be forecast.
655 The results indicate that they were driven by anomalous ocean heat flux convergence but the
656 causes of that are unknown. It would be interesting to identify the wind forcing and changes
657 in currents, mixing and thermocline depth responsible and to also determine if these arise
658 as an occasional part of the ENSO cycle or are a different phenomena, or are influenced by
659 human-driven climate change.

660 The results presented here suggest processes additional to tropical SST-forcing were also
661 involved in generating the west coast ridge, including internal atmosphere variability as

662 argued by Seager et al. (2015), Baxter and Nigam (2015) and Watson et al. (2016) or
663 forcing from other changes in ocean surface conditions (Lee et al. 2015). In terms of any role
664 for climate change it should be noted that the current work indicates that a key feature of the
665 SST anomaly for generating the ridge was warming in the west Pacific relative to the more
666 eastern part of the ocean. That is why Palmer (2014) noted that for anthropogenic climate
667 change to have played a role in the SST states that contributed to the extreme winter of
668 2013/14 it would require a non-uniform SST response to radiative forcing and essentially
669 invoked the ocean dynamical thermostat mechanism of Clement et al. (1996) and Cane
670 et al. (1997). Whether such a dynamically-influenced forced SST change is occurring in
671 nature is unknown but needs to be determined. Whatever the answer, that tropical SST
672 anomalies that are neither El Niño nor La Niña can help create such a dramatic climate
673 anomaly over North America as the west coast ridge of winter 2013/14 is interesting and,
674 now that it is identified, should provide a means to improve seasonal prediction for the
675 continent provided that the SST anomalies can first be monitored with sufficient accuracy
676 and secondly predicted.

677 *Acknowledgments.*

678 This work was supported by NSF awards AGS-1401400 and AGS-1243204 and NOAA
679 award NA14OAR4310232. We thank Mark Cane and Dong-Eun Lee for conversations and
680 additional simulations analyzing sensitivity of circulation anomalies to SST data sets. We
681 also thank three anonymous reviewers for constructive criticisms.

REFERENCES

- 684 Adler, R. F., et al., 2003: The version-2 global precipitation climatology project (GPCP)
685 monthly precipitation analysis (1979-present). *J. Hydrometeor.*, **4**, 1147–1167.
- 686 Alexander, M. A., 1992a: Midlatitude atmosphere-ocean interaction during El Niño. Part I:
687 The North Pacific Ocean. *J. Climate*, **5**, 944–958.
- 688 Alexander, M. A., 1992b: Midlatitude atmosphere-ocean interaction during El Niño. Part
689 II: The northern hemisphere. *J. Climate*, **5**, 959–972.
- 690 Balmaseda, M. A., K. Mogensen, and A. T. Weaver, 2013: Evaluation of the ECMWF ocean
691 reanalysis system ORAS4. *Quart. J. Roy. Meteor. Soc.*, **139**, 1132–1161.
- 692 Baxter, S. and S. Nigam, 2015: Key role of the North Pacific Oscillation-West Pacific Pattern
693 in generating the extreme 2013/14 North American winter. *J. Climate*, **28**, 8109–8117.
- 694 Berrisford, P., P. Kallberg, S. Kobayashi, D. Dee, S. Uppala, A. J. Simmons, P. Poli, and
695 H. Sato, 2011a: Atmospheric conservation properties in ERA-Interim. *Quart. J. Royal
696 Meteor. Soc.*, **137**, 1381–1399.
- 697 Berrisford, P., et al., 2011b: The ERA-Interim archive version 2.0. Tech. rep., European
698 Centre for Medium Range Weather Forecasts, ERA report series No. 1, 23 pp.
- 699 Bond, N. E., M. F. Cronin, H. Freeland, and N. Mantua, 2015: Causes and impacts of the
700 2014 warm anomaly in the NE Pacific. *Geophys. Res. Lett.*, doi:10.1002/2015GL063306.
- 701 Cane, M. A., A. C. Clement, A. Kaplan, Y. Kushnir, D. Pozdnyakov, R. Seager, S. E. Zebiak,
702 and R. Murtugudde, 1997: Twentieth Century sea surface temperature trends. *Science*,
703 **275**, 957–960.
- 704 Cayan, D., 1992: Latent and sensible heat flux anomalies over the northern oceans: Driving
705 the sea surface temperature. *J. Phys. Oceanogr.*, **22**, 859–881.

706 Clement, A. C., R. Seager, M. A. Cane, and S. E. Zebiak, 1996: An ocean dynamical
707 thermostat. *J. Climate*, **9**, 2190–2196.

708 Copsey, D., R. Sutton, and J. R. Knight, 2006: Recent trends in sea level pressure in the
709 Indian Ocean region. *Geophys. Res. Lett.*, **33**, L19 712,doi:10.1029/2006GL027 175.

710 Davies, H. C., 2015: Weather chains during the 2013/14 winter and their significance for
711 seasonal prediction. *Nature Geo.*, **8**, 833–837.

712 Dee, D., et al., 2011: The ERA-Interim Reanalysis; Configuration and performance of the
713 data assimilation system. *Quart. J. Roy. Meteor. Soc.*, **137**, 553–597.

714 Funk, C., A. Hoell, and D. Stone, 2014: Examining the contribution of the observed global
715 warming trend to the California droughts of 2012/13 and 2013/14. (In Explaining Extremes
716 of 2013 from a Climate Perspective). *Bull. Amer. Meteor. Soc.*, **95**, S11–S15.

717 Gill, A. E., 1980: Some simple solutions for heat induced tropical circulation. *Quart. J. Roy.*
718 *Meteorol. Soc.*, **106**, 447–462.

719 Harnik, N., R. Seager, N. Naik, M. Cane, and M. Ting, 2010: The role of linear wave
720 refraction in the transient eddy-mean flow response to tropical Pacific SST anomalies.
721 *Quart. J. Roy. Meteor. Soc.*, 2132–2146.

722 Hartmann, D. L., 2015: Pacific sea surface temperature and the winter of 2014. *Geophys.*
723 *Res. Lett.*, **42**, doi:10.1002/2015GL063 083.

724 Herring, S. C., M. P. Hoerling, T. C. Peterson, and P. A. Stott, 2014: Explaining extreme
725 events of 2013 from a climate perspective. *Bull. Amer. Meteor. Soc.*, **95**, S1–S96.

726 Hoerling, M. P., J. W. Hurrell, and T. Xu, 2001: Tropical origins for recent North Atlantic
727 climate change. *Science*, **292**, 90–92.

728 Hoskins, B. and K. Karoly, 1981: The steady response of a spherical atmosphere to thermal
729 and orographic forcing. *J. Atmos. Sci.*, **38**, 1179–1196.

- 730 Howitt, R. E., J. Medellin-Azuara, D. MacEwan, J. R. Lund, and D. A. Summer, 2014:
731 Economic Analysis of the 2014 Drought for California Agriculture. Tech. rep., Center for
732 Watershed Sciences, University of California, Davis, California, 20 pp.
- 733 Huang, B., et al., 2015: Extended reconstructed sea surface temperature version 4
734 (ERSST.v4). Part I: Upgrades and intercomparisons. *J. Climate*, **28**, 911–930.
- 735 Huffman, G. J. et al., 1997: The Global Precipitation Climatology Project (GPCP) Com-
736 bined Precipitation Dataset. *Bull. Amer. Meteor. Soc.*, **78**, 5–20.
- 737 Kiehl, J. T., J. J. Hack, G. B. Bonan, B. A. Bovile, D. L. Williamson, and P. J. Rasch, 1998:
738 The National Center for Atmospheric Research Community Climate Model: CCM3. *J.*
739 *Climate*, **11**, 1131–1149.
- 740 Kistler, R., et al., 2001: The NCEP-NCAR 50-year Reanalysis: Monthly means CD-ROM
741 and documentation. *Bull. Am. Meteor. Soc.*, **82**, 247–268.
- 742 Lau, N.-C. and M. J. Nath, 1994: A modeling study of the relative roles of tropical and
743 extratropical SST anomalies in the variability of the global atmosphere-ocean system. *J.*
744 *Climate*, **7**, 1184–1207.
- 745 Lau, N.-C. and M. J. Nath, 1996: The role of the ‘atmospheric bridge’ in linking tropical
746 Pacific ENSO events to extratropical SST anomalies. *J. Climate*, **9**, 2036–2057.
- 747 Lee, M., C. Hong, and H. Hsu, 2015: Compounding effects of warm sea surface tem-
748 perature and reduced sea ice on the extreme circulation over the extratropical North
749 Pacific and North America during the 2013-14 boreal winter. *Geophys. Res. Lett.*,
750 doi:10.1002/2014GL062956.
- 751 Palmer, T. N., 2014: Record breaking winters and global climate change. *Science*, **344**,
752 803–4.
- 753 Rayner, N., D. Parker, E. Horton, C. Folland, L. Alexander, D. Rowell, E. Kent, and A. Ka-
754 plan, 2003: Global analyses of sea surface temperature, sea ice, and night marine air tem-
755 perature since the late nineteenth century. *J. Geophys. Res.*, **108**, 10.1029/2002JD002670.

- 756 Sardeshmukh, P. D. and B. J. Hoskins, 1988: The generation of global rotational flow by
757 steady idealized tropical divergence. *J. Atmos. Sci.*, **45**, 1228–1251.
- 758 Seager, R., L. Goddard, J. Nakamura, N. Naik, and D. Lee, 2014a: Dynamical causes of the
759 2010/11 Texas-northern Mexico drought. *J. Hydromet.*, **15**, 39–68.
- 760 Seager, R., N. Harnik, Y. Kushnir, W. Robinson, and J. Miller, 2003: Mechanisms of hemi-
761 spherically symmetric climate variability. *J. Climate*, **16**, 2960–2978.
- 762 Seager, R., M. Hoerling, S. Schubert, H. Wang, B. Lyon, A. Kumar, J. Nakamura, and
763 N. Henderson, 2015: Causes of the 2011-14 California drought. *J. Climate*, **28**, 6997–7024.
- 764 Seager, R., Y. Kushnir, C. Herweijer, N. Naik, and J. Velez, 2005: Modeling of tropical
765 forcing of persistent droughts and pluvials over western North America: 1856-2000. *J.*
766 *Climate*, **18**, 4068–4091.
- 767 Seager, R., N. Naik, W. Baethgen, A. Robertson, Y. Kushnir, J. Nakamura, and S. Jurburg,
768 2010a: Tropical oceanic causes of interannual to multidecadal precipitation variability in
769 southeast South America over the past century. *J. Climate*, **23**, 5517–5539.
- 770 Seager, R., N. Naik, M. A. Cane, N. Harnik, M. Ting, and Y. Kushnir, 2010b: Adjustment
771 of the atmospheric circulation to tropical Pacific SST anomalies: Variability of transient
772 eddy propagation in the Pacific-North America sector. *Quart. J. Roy. Meteorol. Soc.*,
773 **136**, 277–296.
- 774 Seager, R., D. Neelin, I. Simpson, H. Liu, N. Henderson, T. Shaw, Y. Kushnir, and M. Ting,
775 2014b: Dynamical and thermodynamical causes of large-scale changes in the hydrological
776 cycle over North America in response to global warming. *J. Climate*, **27**, 7921–7948.
- 777 Seager, R., et al., 2009: Mexican drought: An observational, modeling and tree ring study
778 of variability and climate change. *Atmosfera*, **22**, 1–31.
- 779 Swain, D., M. Tsiang, M. Haughen, D. Singh, A. Charland, B. Rajarthan, and N. S. Diff-
780 enbaugh, 2014: The extraordinary California drought of 2013/14: Character, context and

781 the role of climate change. (In Explaining Extremes of 2013 from a Climate Perspective).
782 *Bull. Amer. Meteor. Soc.*, **95**, S3–S6.

783 Trenberth, K., G. W. Branstator, D. Karoly, A. Kumar, N. Lau, and C. Ropelewski, 1998:
784 Progress during TOGA in understanding and modeling global teleconnections associated
785 with tropical sea surface temperature. *J. Geophys. Res.*, **103**, 14 291–14 324.

786 Wang, H. and S. Schubert, 2014: Causes of the extreme dry conditions over California
787 during early 2013. (In Explaining Extremes of 2013 from a Climate Perspective). *Bull.*
788 *Amer. Meteor. Soc.*, **95**, S7–S10.

789 Watson, P. A. G., A. Weisheimer, J. R. Knight, and T. N. Palmer, 2016: The role of the
790 tropical West Pacific in the extreme northern hemisphere winter of 2013/14. *J. Geophys.*
791 *Res.*, **121**, 1698–1714.

792 Williams, A. P., et al., 2015: Correlations between components of the water balance and
793 burned area reveal new insights for predicting forest-fire area in the southwest United
794 States. *Int. J. Wildland Fire*, **24**, 14–26.

795 Yu, L., X. Jin, and R. Weller, 2008: Multidecade global flux datasets from the Objectively
796 Analyzed Air-sea Fluxes (OAFlux) Project: Latent and sensible heat fluxes, ocean evapo-
797 ration, and related surface meteorological variables. Tech. rep., Woods Hole Oceanographic
798 Institute OAFlux Project OA-2008-01, 64pp. Woods Hole. Massachusetts., 64 pp.

799 List of Figures

- 800 1 The 200mb height (meters) and precipitation anomalies (mm/month) from
801 the NCEP-NCAR (upper left) and ERA-Interim (upper right) Reanalyses,
802 ERSSTv4 SST (Kelvin) and OA surface latent plus sensible surface heat flux
803 (positive into the ocean, W/m^2) anomalies (middle left) and NCEP high pass
804 filtered 200mb meridional velocity variance anomaly (m^2/s^2 , middle right) and
805 GPCP (lower left) and CPC CMAP (lower right) satellite-gauge precipitation
806 anomalies (mm/month) all for DJF 2013/14. 34
- 807 2 The observed DJF 2013/14 SST anomalies (left column) from the Hadley
808 (top), ORAS4 (middle) and ERSSTv4 (bottom) data sets and the 100 member
809 ensemble mean 200mb height (contours) and precipitation (colors) response
810 of CCM3 (middle column) and CAM5 (right column) to these when imposed
811 on the same SST climatology. Units are Kelvin for SST, meters for height
812 and mm/day for precipitation. For the height fields, the contour interval is
813 10m with the zero contour suppressed. 35
- 814 3 The imposed “box-SST anomalies” (left column) and the 100 member ensem-
815 ble mean 200mb height response (right column). The SST anomalies were
816 imposed upon a DJF SST climatology and the average is over days 40-100 of
817 100 day simulations initiated on December 1st. In the left column the mod-
818 eled land surface temperature response is also shown. Units are Kelvin for
819 temperature and meters for height. 36

- 820 4 The ERSSTv4 observed SST anomaly (top left) and the GPCP observed
821 precipitation (colors, top right) and NCEP 200mb height (contours, top right)
822 anomalies for DJF 2013/14. The middle row shows the equivalents, plus
823 modeled land surface temperature response, constructed by the optimal sum
824 of the “box-SST anomaly” forcing experiments and the bottom row shows
825 the same but for the single ensemble forced by the corresponding constructed
826 SST anomaly. Units are Kelvin for SST, meters for height and mm/day for
827 precipitation. 37
- 828 5 The high pass filtered 200mb meridional velocity variance for the “box-SST
829 anomalies” experiments. The SST anomalies are shown in Figure 3 and their
830 location indicated here by the boxes. The meridional velocity variances were
831 averaged over days 40-100 of 100 day simulations initiated on December 1st.
832 Units are m^2/s^2 . 38
- 833 6 The 200mb height anomaly (left) and high pass filtered 200mb meridional
834 velocity variance (right) for responses to the optimal SST anomaly at different
835 times following switch-on of the anomaly. Units are m for height and m^2/s^2
836 for velocity variance. 39
- 837 7 The terms in the 200mb vorticity budget from the NCEP-NCAR Reanalysis
838 averaged over DJF 2013/14. Units are s^{-2} and terms have been multiplied by
839 10^6 for plotting purposes. 40
- 840 8 Same as Figure 7 but for the 100 member ensemble mean of the last 60 days
841 of the model simulations of the response to the optimal SST pattern. 41
- 842 9 The NCEP Reanalysis winter 2013/14 (left) and 100 member ensemble mean
843 of the last 60 days of the model simulations of the response to the optimal
844 SST pattern (right), anomalous divergent wind (m/s) and velocity potential
845 (s^{-1} , multiplied by 10^6) (top) and anomalous surface pressure over ocean (Pa ,
846 bottom). 42

- 847 10 Day 5 (top), 11 (middle) and 17 (bottom) snapshots of the transient evolution
848 of the leading terms in the vorticity budget of the 100 member ensemble mean
849 of the optimal SST anomaly switch-on experiments. Units are s^{-2} and terms
850 have been multiplied by 10^6 for plotting purposes. 43
- 851 11 As for Figure 9 but for the rotational and divergent components of the zonal
852 (left) and meridional (right) flow anomalies. Units are m/s . For plotting
853 purposes contours and colors corresponding to more than 5 m/s are not shown. 44
- 854 12 The 200mb height and precipitation anomaly for the four optimal SST anomaly
855 perturbed ensemble members that have the highest extratropical pattern cor-
856 relation with the observed DJF 2013/14 height anomaly. Units are m/s for
857 heights and mm/day for precipitation. Bottom, the histograms of pattern
858 correlation coefficients between the extratropical height anomalies of the en-
859 semble members and the observed DJF 2013/14 anomaly for (left) the control
860 ensemble and (right) the optimized SST anomaly perturbed ensemble. 45

Observed DJF 2013-2014 anomalies

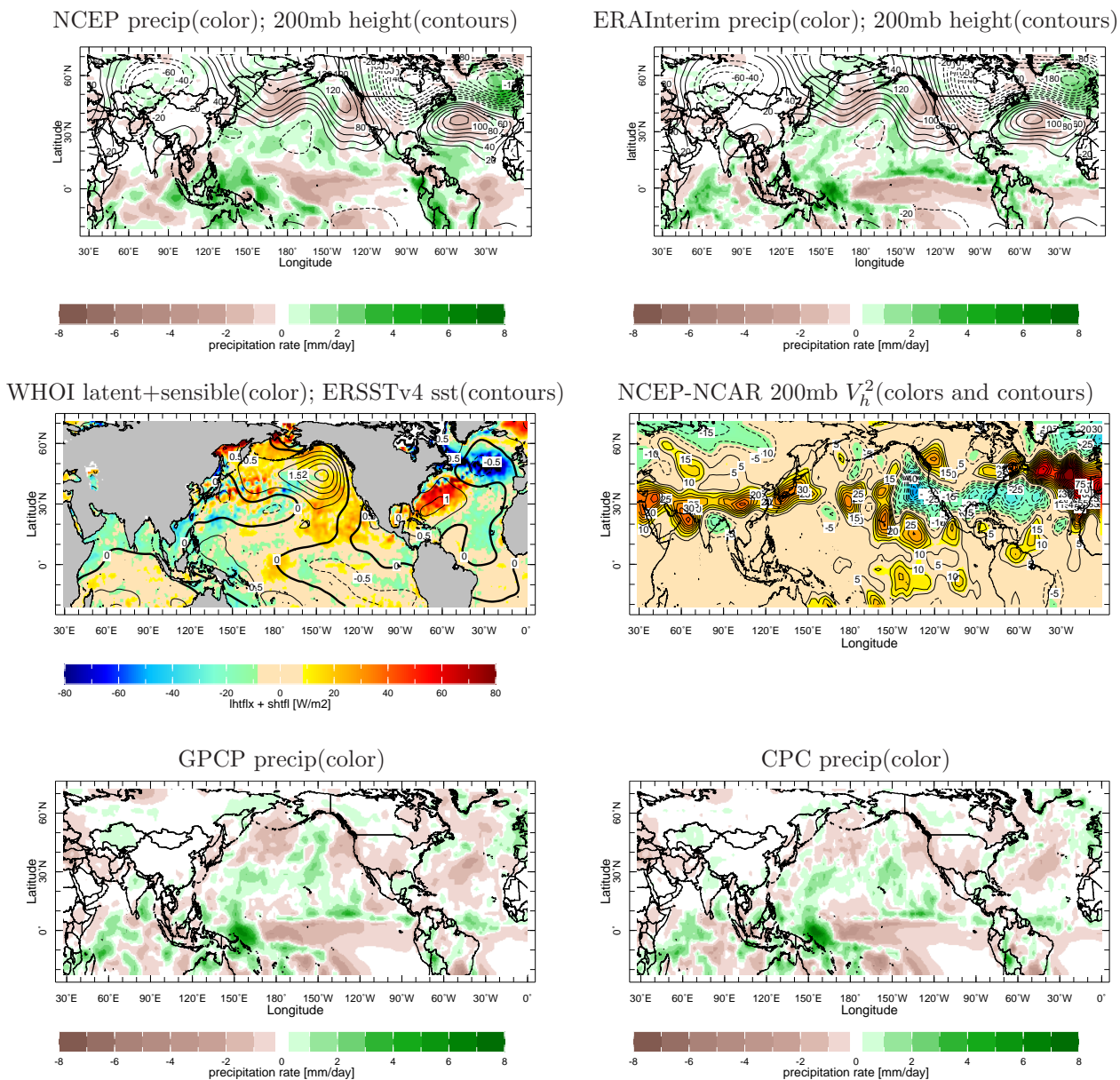


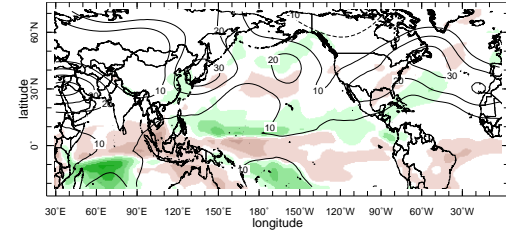
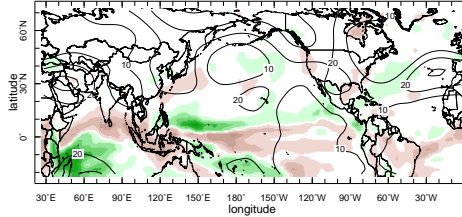
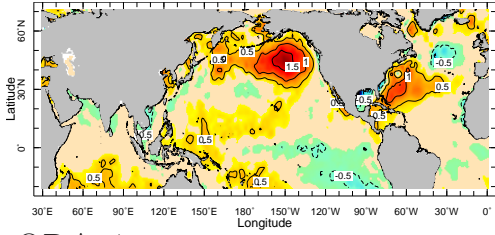
FIG. 1. The 200mb height (meters) and precipitation anomalies (mm/month) from the NCEP-NCAR (upper left) and ERA-Interim (upper right) Reanalyses, ERSSTv4 SST (Kelvin) and OA surface latent plus sensible surface heat flux (positive into the ocean, W/m^2) anomalies (middle left) and NCEP high pass filtered 200mb meridional velocity variance anomaly (m^2/s^2 , middle right) and GPCP (lower left) and CPC CMAP (lower right) satellite-gauge precipitation anomalies (mm/month) all for DJF 2013/14.

DJF 2013/14 SST anomalies

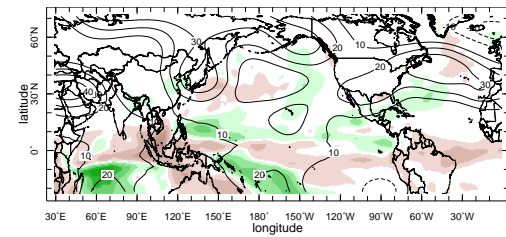
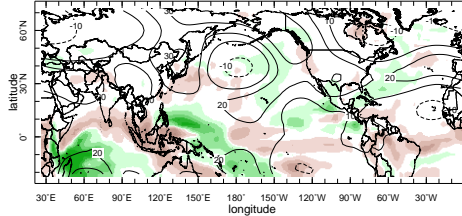
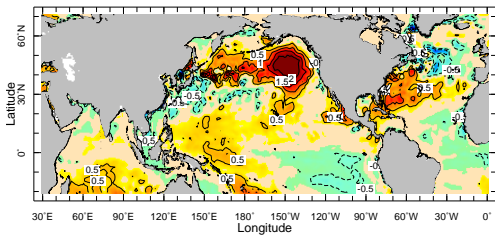
CCM3.10 response

CAM5.3 response

Hadley



ORAs4



ERSSTv4

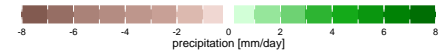
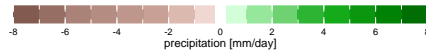
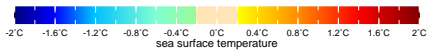
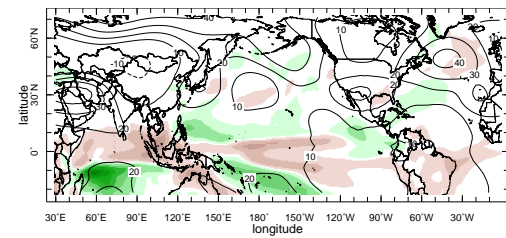
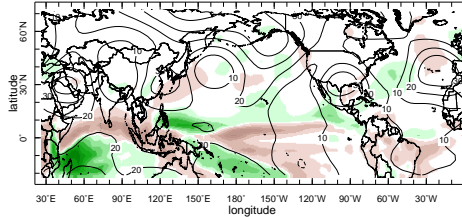
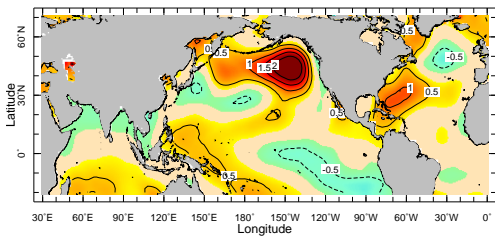


FIG. 2. The observed DJF 2013/14 SST anomalies (left column) from the Hadley (top), ORAs4 (middle) and ERSSTv4 (bottom) data sets and the 100 member ensemble mean 200mb height (contours) and precipitation (colors) response of CCM3 (middle column) and CAM5 (right column) to these when imposed on the same SST climatology. Units are Kelvin for SST, meters for height and mm/day for precipitation. For the height fields, the contour interval is 10m with the zero contour suppressed.

SSTA forcing and land surface
temperature response

200mb height response

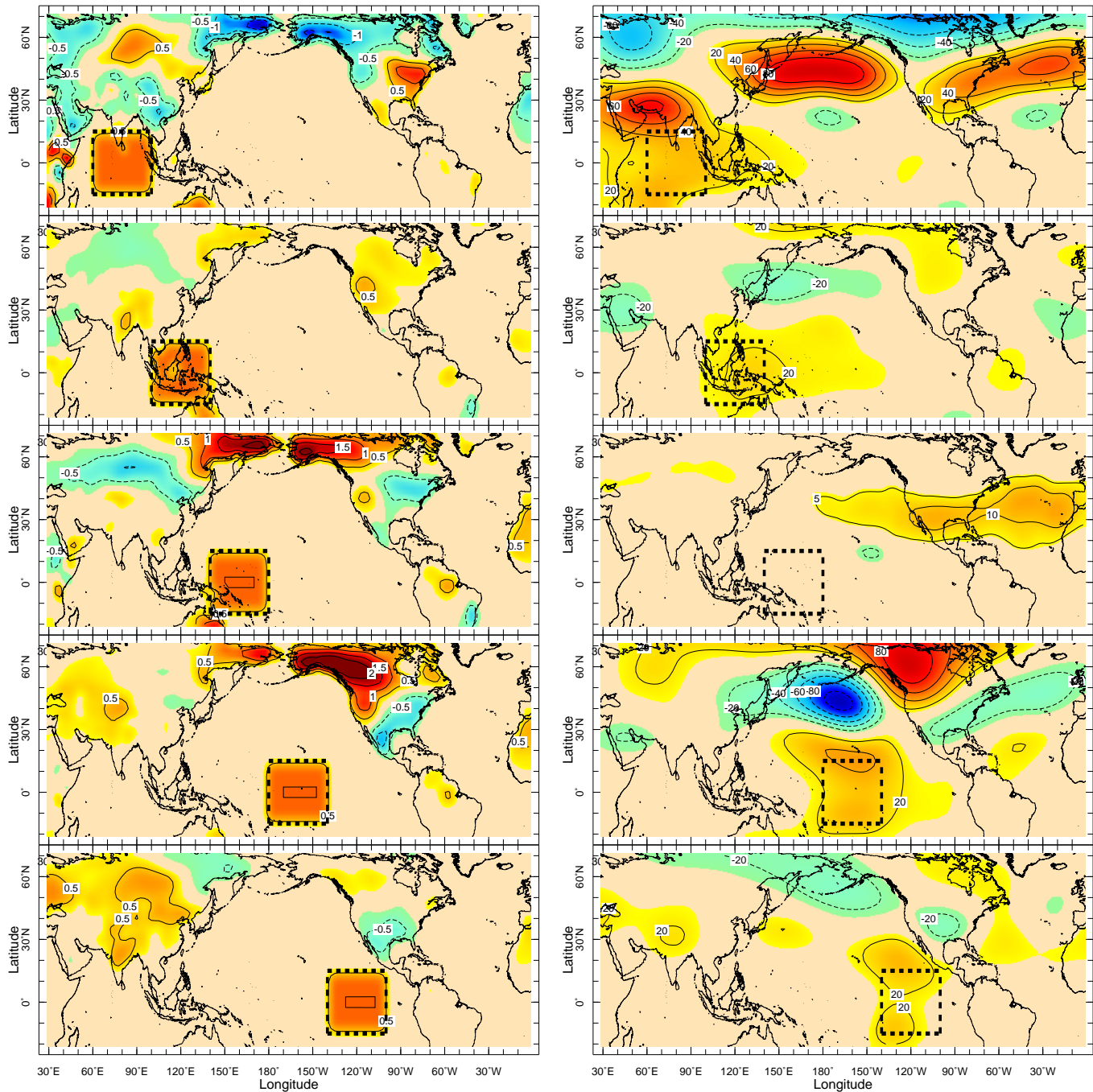
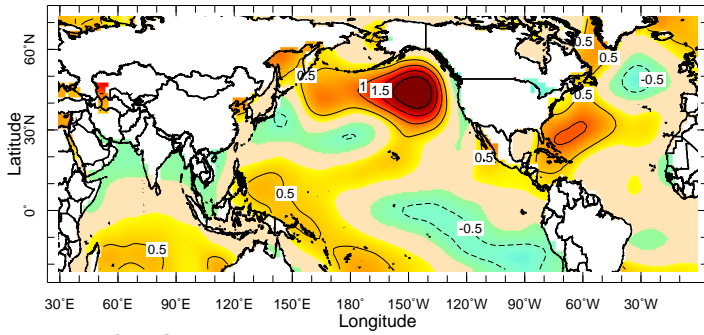
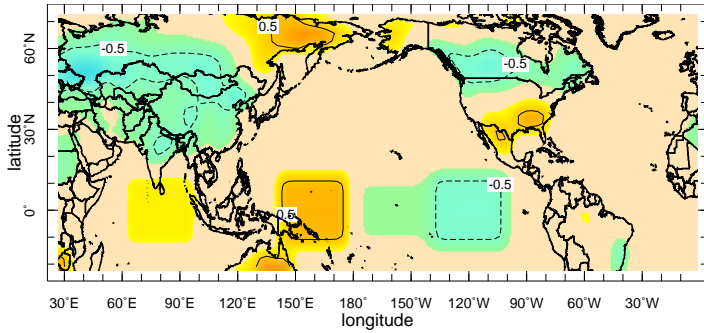


FIG. 3. The imposed “box-SST anomalies” (left column) and the 100 member ensemble mean 200mb height response (right column). The SST anomalies were imposed upon a DJF SST climatology and the average is over days 40-100 of 100 day simulations initiated on December 1st. In the left column the modeled land surface temperature response is also shown. Units are Kelvin for temperature and meters for height.

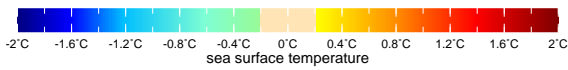
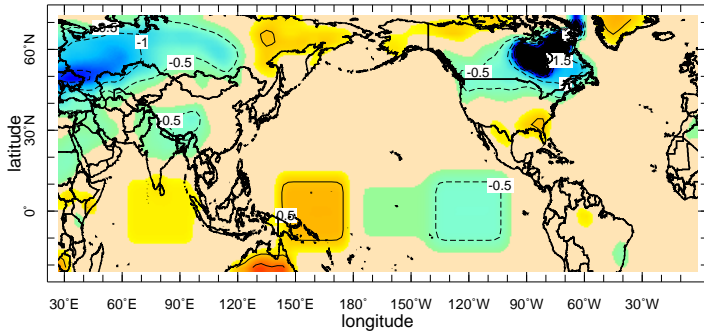
ERSSTv4



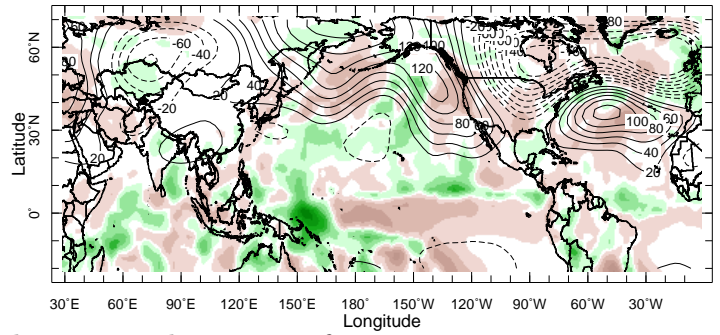
optimal 5 boxes



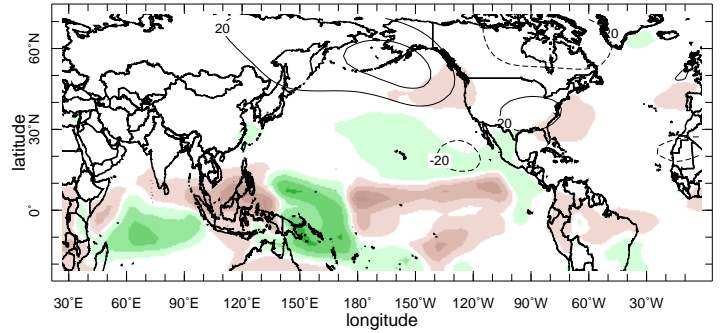
optimal 5 boxes



GPCP/NCEP-NCAR



linear combination of responses



response to linear combination

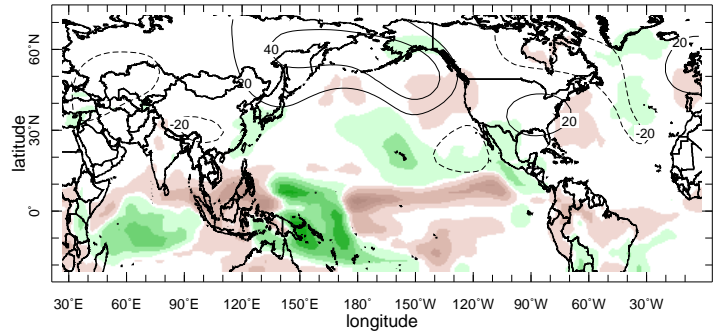


FIG. 4. The ERSSTv4 observed SST anomaly (top left) and the GPCP observed precipitation (colors, top right) and NCEP 200mb height (contours, top right) anomalies for DJF 2013/14. The middle row shows the equivalents, plus modeled land surface temperature response, constructed by the optimal sum of the “box-SST anomaly” forcing experiments and the bottom row shows the same but for the single ensemble forced by the corresponding constructed SST anomaly. Units are Kelvin for SST, meters for height and mm/day for precipitation.

anomalous 200mb VhVh

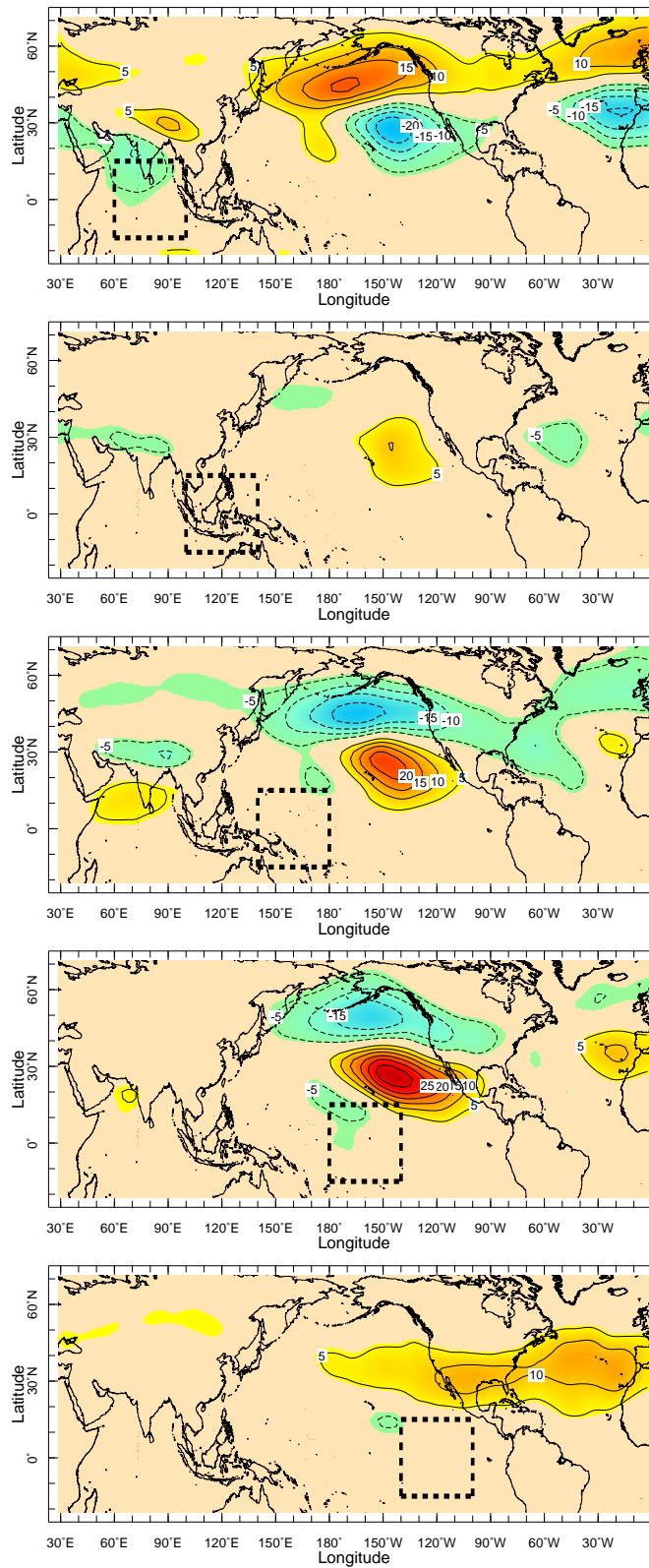


FIG. 5. The high pass filtered 200mb meridional velocity variance for the “box-SST anomalies” experiments. The SST anomalies are shown in Figure 3 and their location indicated here by the boxes. The meridional velocity variances were averaged over days 40-100 of 100 day simulations initiated on December 1st. Units are m^2/s^2 .

Response to optimal SST

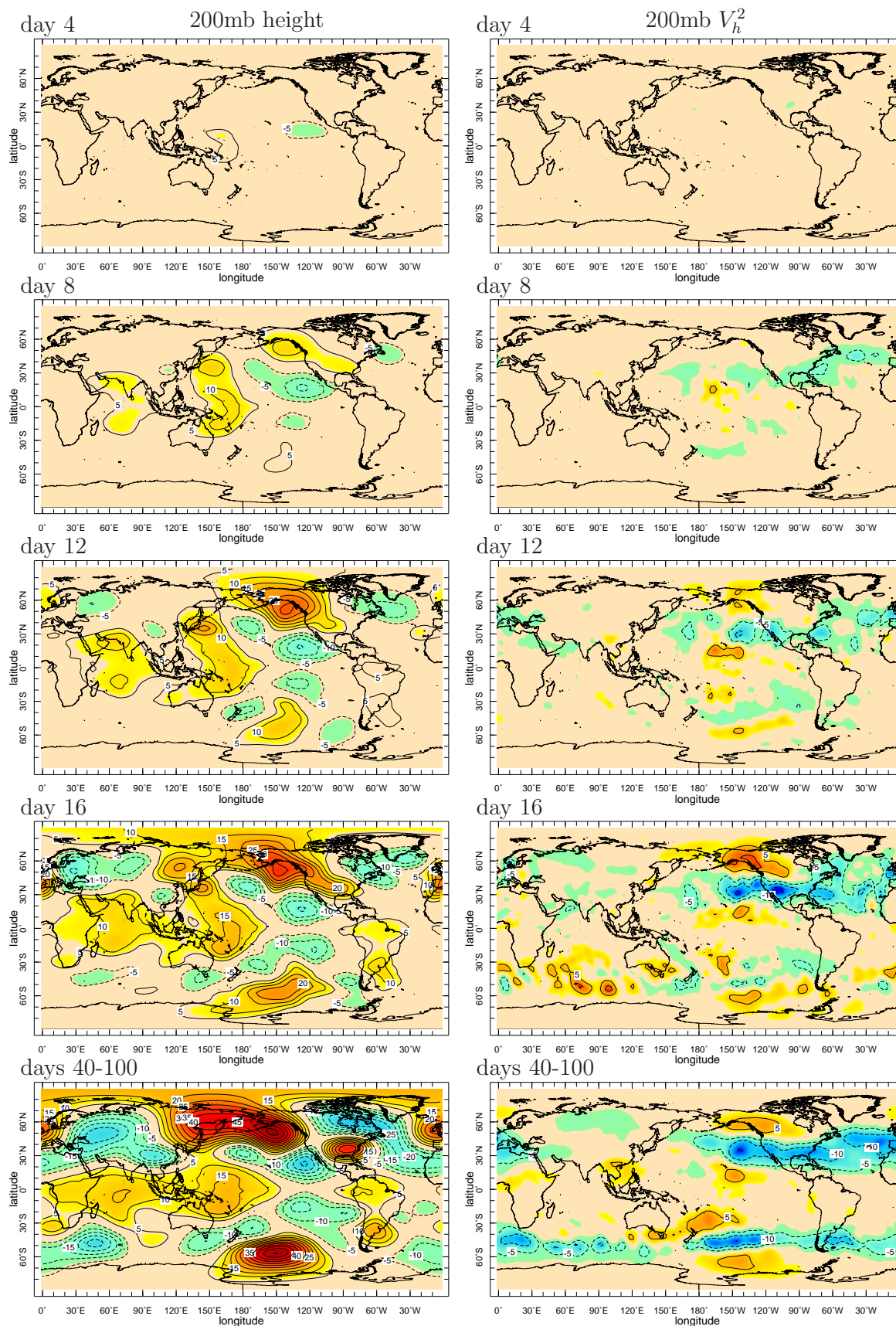


FIG. 6. The 200mb height anomaly (left) and high pass filtered 200mb meridional velocity variance (right) for responses to the optimal SST anomaly at different times following switch-on of the anomaly. Units are m for height and m^2/s^2 for velocity variance.

NCEP-NCAR 200mb vorticity budget, DJF2013-14 anomalies

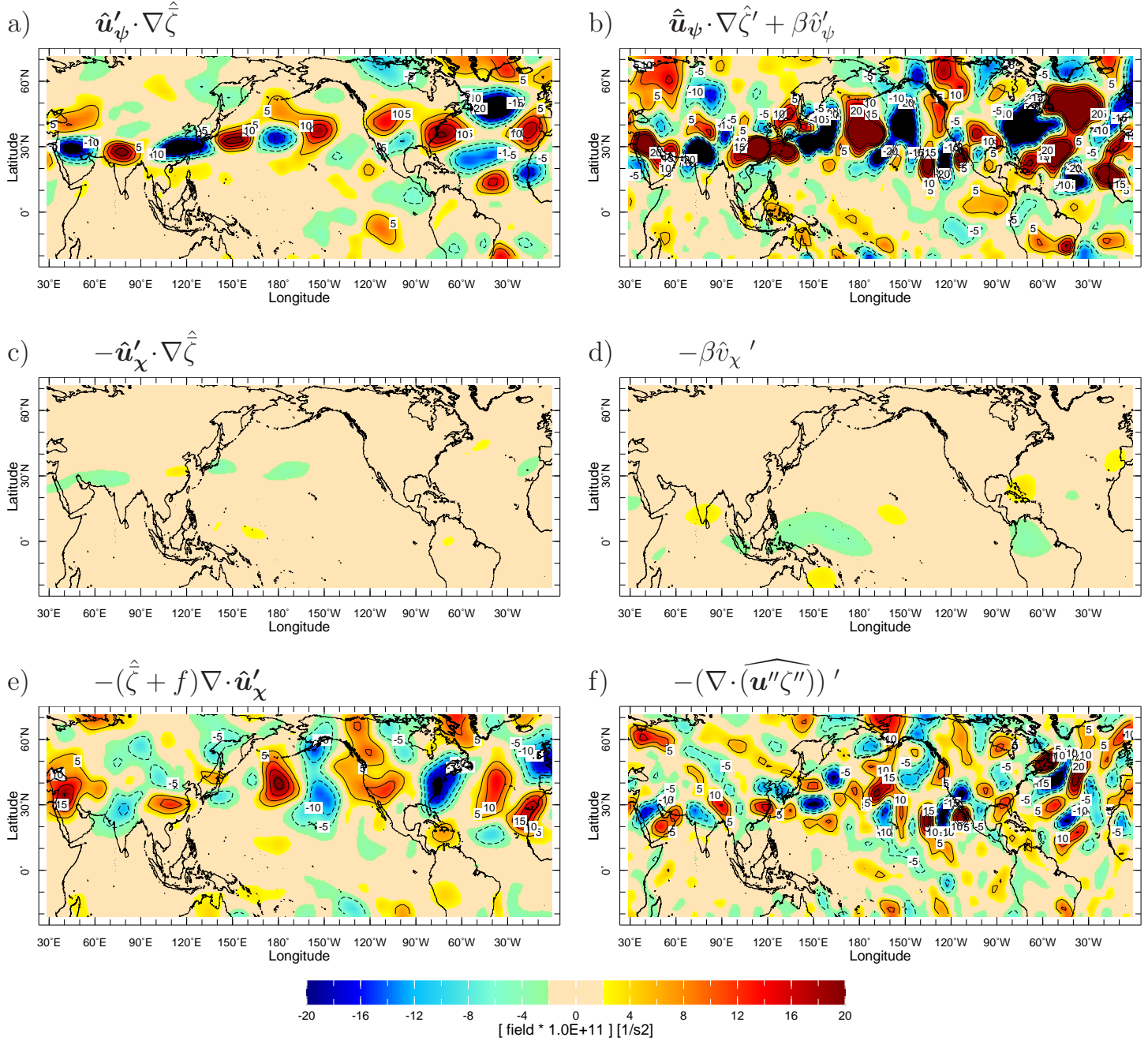


FIG. 7. The terms in the 200mb vorticity budget from the NCEP-NCAR Reanalysis averaged over DJF 2013/14. Units are s^{-2} and terms have been multiplied by 10^6 for plotting purposes.

Anomalous response to optimal SST pattern, 200mb vorticity budget

mean of last 60 days

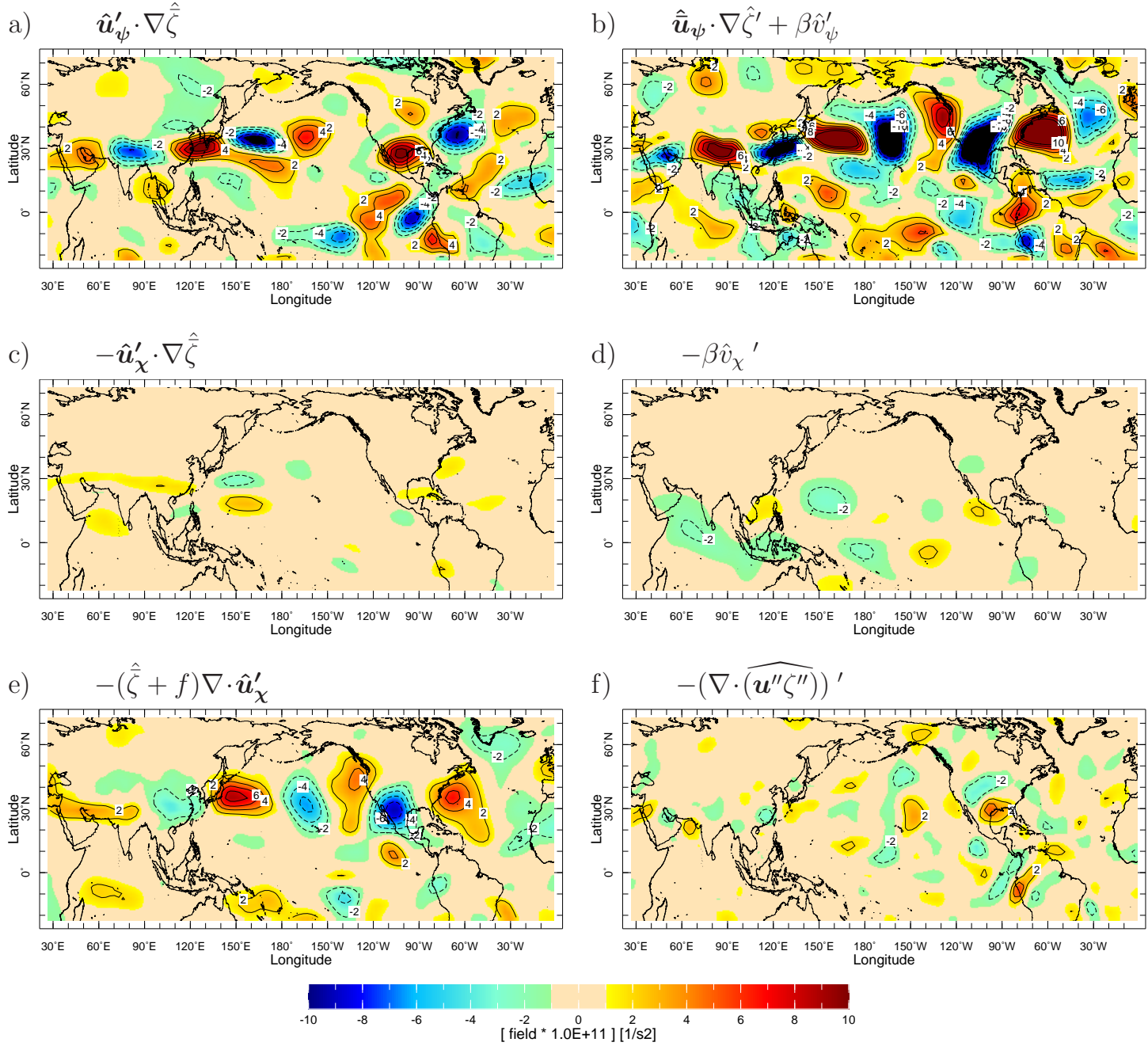
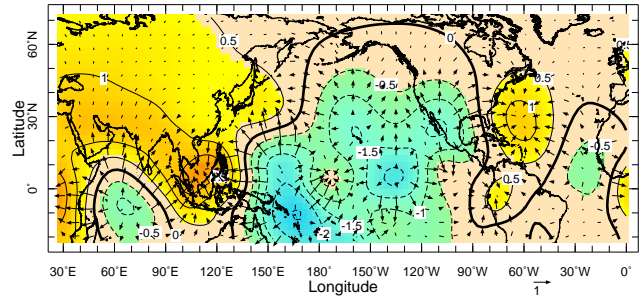
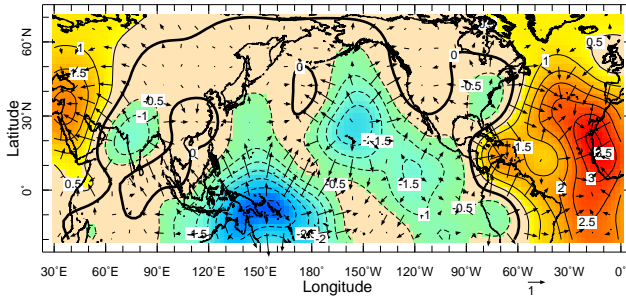


FIG. 8. Same as Figure 7 but for the 100 member ensemble mean of the last 60 days of the model simulations of the response to the optimal SST pattern.

Anomalous 200mb velocity potential (color/contours), divergent winds (vectors)

NCEP

response to optimal SST pattern



Surface pressure anomalies

NCEP

response to optimal SST pattern

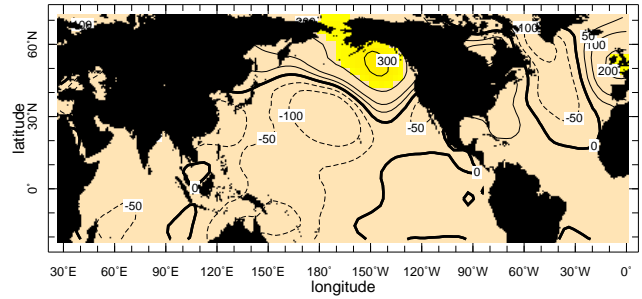
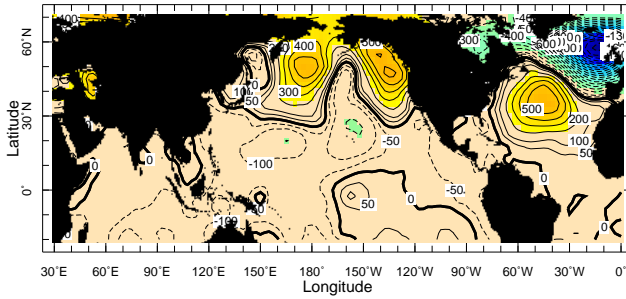
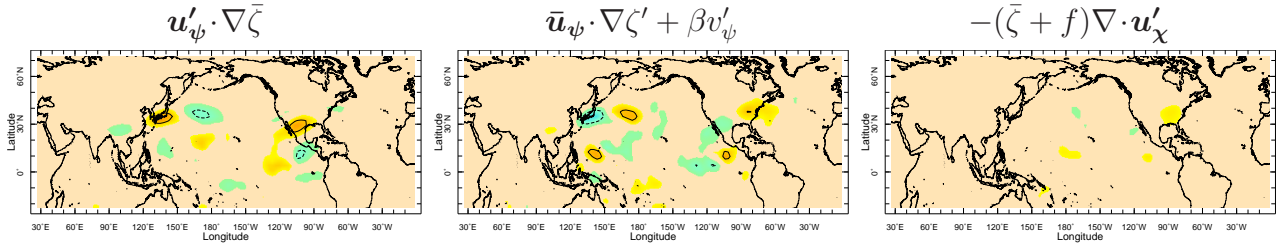


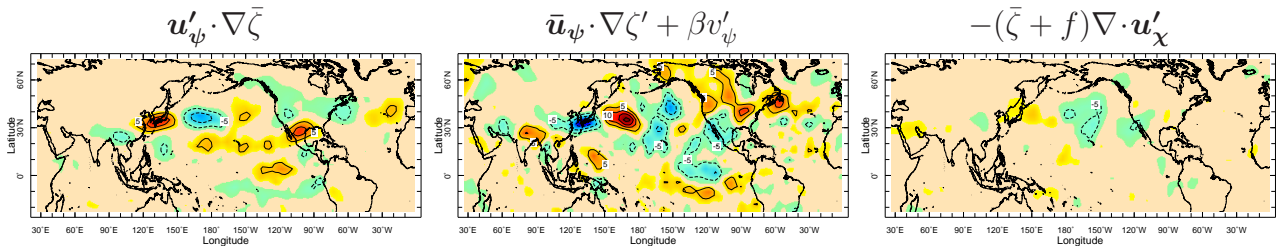
FIG. 9. The NCEP Reanalysis winter 2013/14 (left) and 100 member ensemble mean of the last 60 days of the model simulations of the response to the optimal SST pattern (right), anomalous divergent wind (m/s) and velocity potential (s^{-1} , multiplied by 10^6) (top) and anomalous surface pressure over ocean (Pa , bottom).

Anomalous response to optimal SST pattern, 200mb vorticity budget

day 5



day 11



day 17

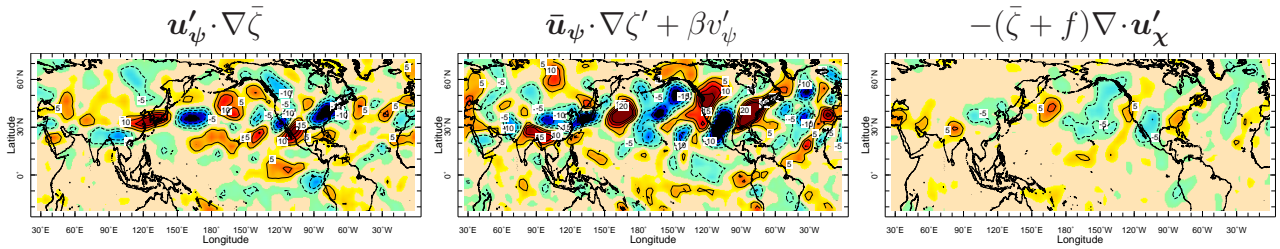


FIG. 10. Day 5 (top), 11 (middle) and 17 (bottom) snapshots of the transient evolution of the leading terms in the vorticity budget of the 100 member ensemble mean of the optimal SST anomaly switch-on experiments. Units are s^{-2} and terms have been multiplied by 10^6 for plotting purposes.

Anomalous response to optimal SST pattern, 200mb vorticity budget

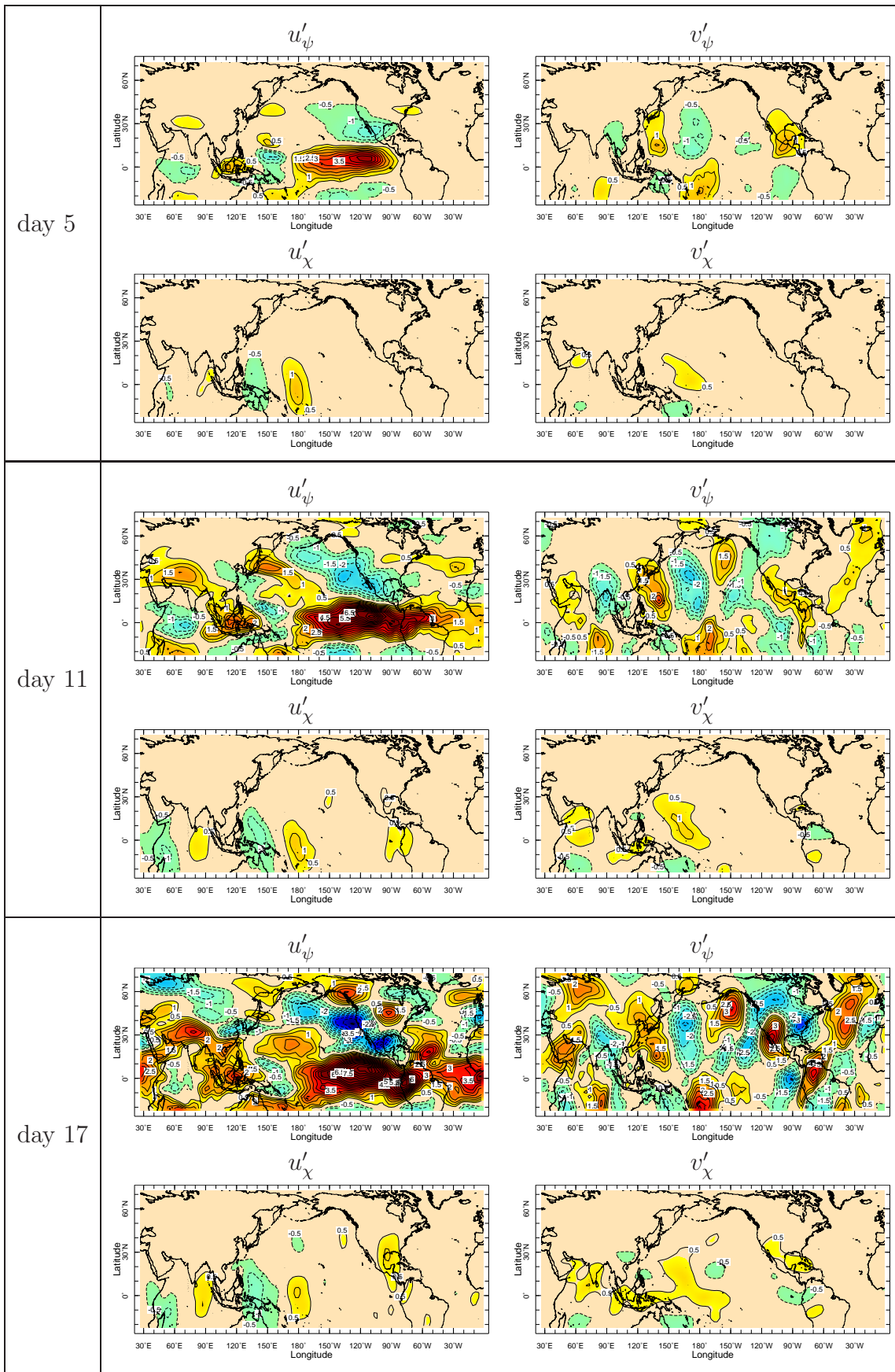
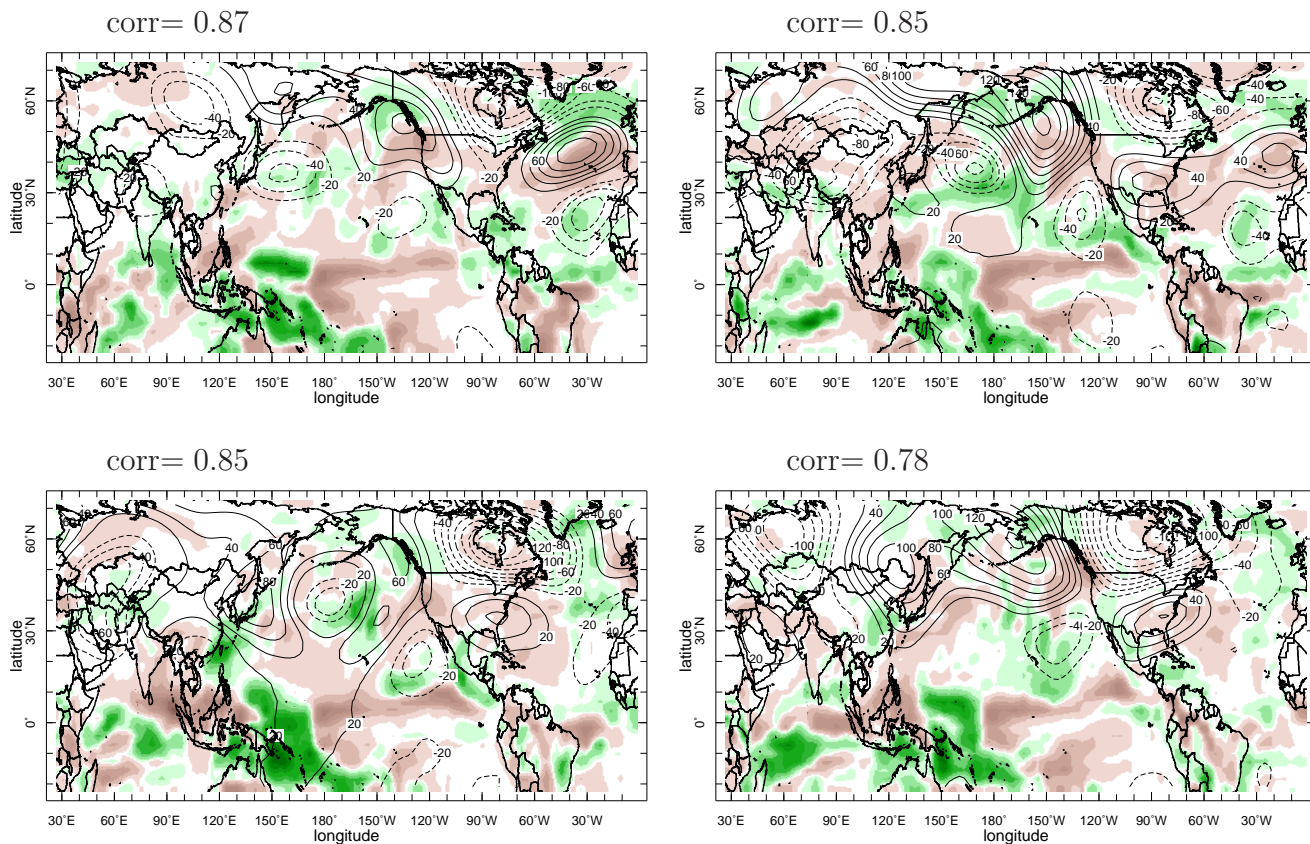


FIG. 11. As for Figure 9 but for the rotational and divergent components of the zonal (left) and meridional (right) flow anomalies. Units are m/s . For plotting purposes contours and colors corresponding to more than 5 m/s are not shown.

top four ensemble members



pattern correlations

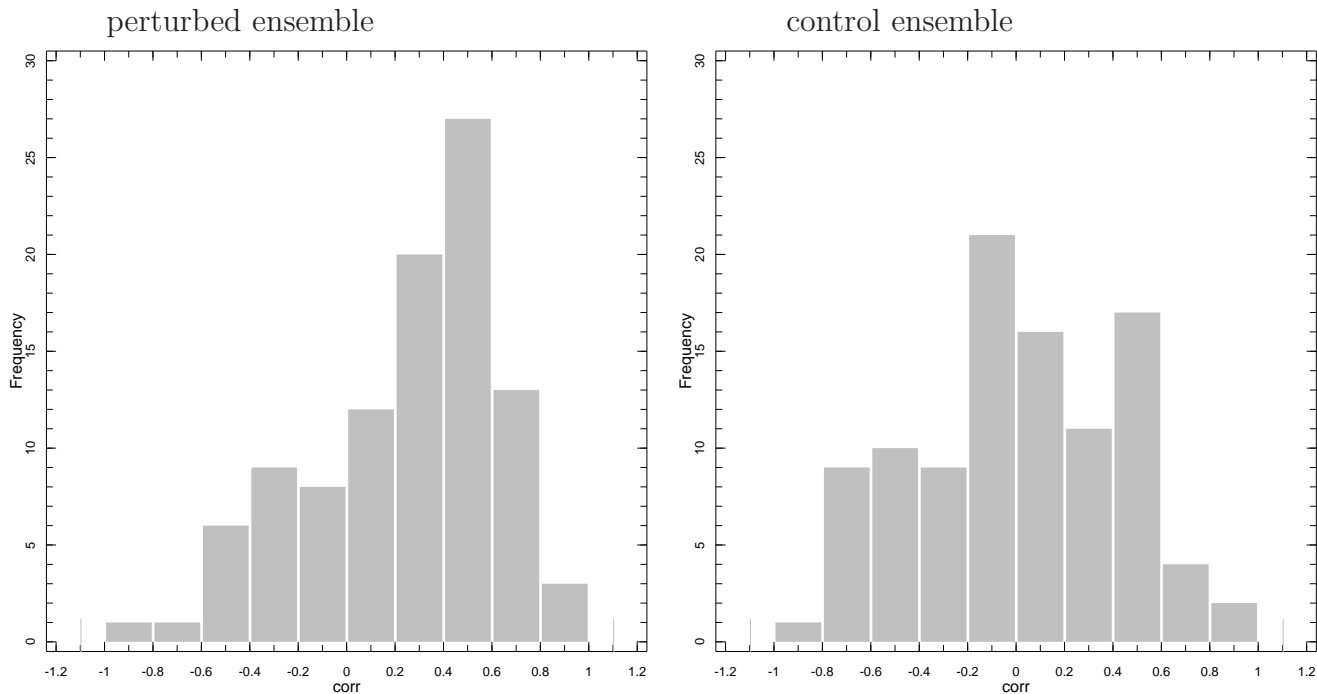


FIG. 12. The 200mb height and precipitation anomaly for the four optimal SST anomaly perturbed ensemble members that have the highest extratropical pattern correlation with the observed DJF 2013/14 height anomaly. Units are m/s for heights and mm/day for precipitation. Bottom, the histograms of pattern correlation coefficients between the extratropical height anomalies of the ensemble members and the observed DJF 2013/14 anomaly for (left) the control ensemble and (right) the optimized SST anomaly perturbed ensemble.